nature communications

Article

https://doi.org/10.1038/s41467-026-70858-6

CXCR5$^+$ monocyte emigration impairs the radiation-induced antitumor immune response

Received: 11 April 2025

Accepted: 9 March 2026

Published online: 19 March 2026

Check for updates

Yutiantian Lei[1,2,14], Rui Jia[1,2,14], Chen Chen[2,14], Peihai Cao[2], Jiahong Shi[2], Mengdi Huang[2], Qiuyu Mu[2], Yixin Wang[1], Dairu Hou[2], Mingjun Si[2], Ruishan Guo[1], Jiahao Sun[1], Dingge Jiang[2], Yihan Wang[1], Tingting Lv[3], Ruiying Wang[2], Junyi Zhang[1], Du Yang[1], Hanmin Tang[1], Jianan Li[1], Liuyi Yang[4], Renyi Ding[2,5], Wenhua Li[2,5], Haiyan Liu[2,5], Anjun Jiao[2], Lingyun Hui[6], Yanxia Sui[7], Shan Huang[8], Mengjiao Cai[1], Chenchen He[1], Chen Lin[9], Fei Wang[1,10], Jinlu Ma[1] ✉, Suxia Han[1,11] ✉ & Yuzhu Hou[2,12,13] ✉

A substantial portion of patients experience radioresistance, which impedes clinical benefit. The radiation-induced 'protumor' immune response is previously demonstrated to limit antitumor efficacy. However, the detailed mechanism remains to be explored. In this study, we observe CXCR5$^+$ monocytes are enriched in tumor upon radiation. CXCR5 expression on monocytes in host is induced by tumor-derived VEGF through PI3K/mTOR/HIF-1α axis. Local radiation enhances CXCL13 expression from tumor cells, a specific ligand of CXCR5, which leads to the recruitment of CXCR5$^+$ monocytes. Tumor-infiltrating CXCR5$^+$ monocytes induce radioresistance by inhibiting CD8$^+$ T cells through PD-1/PD-L1 interaction. Moreover, radiation-induced GM-CSF promotes the differentiation of CXCR5$^+$ monocytes toward M2-like macrophages. In contrast, inhibiting VEGFR signaling, neutralizing CXCL13 and GM-CSF, or blocking PD-L1 facilitates radiation-induced tumor control by abrogating CXCR5$^+$ monocyte-mediated immunosuppression. Furthermore, the CXCR5$^+$ and CD14$^+$ populations are increased in patients with cancer following radiotherapy. Monocyte is increased in the peripheral blood of patients with progressive disease following radiotherapy. These findings suggest potential strategies for blocking the CXCR5/CXCL13 axis to improve radiotherapy efficacy.

Radiotherapy (RT) is widely applied as an effective cytotoxic therapy for cancer treatment. More than 50% of patients with tumors require radiation therapy[1–4]. Despite its extensive use in oncotherapy, the weakened effectiveness of RT, such as locoregional recurrence following treatment, occurs in some patients and leads to a worse prognosis[5,6]. Thus, radioresistance-induced therapeutic failure has become the main concern in cancer management. The immune system is recognized for its crucial role in the efficacy of RT[7]. Nevertheless, the immunological mechanism of radioresistance is unclear.

Neoantigens, cytokines, and chemokines are released in tumor tissue following ionizing radiation (IR) exposure. These signals aroused immune response, typically the activation of cytotoxic T cells, which is required for the full antitumor effect of RT[8]. In addition to "antitumor" immune responses, radiotherapy elicits "protumor"

A full list of affiliations appears at the end of the paper. ✉e-mail: majinlu@xjtufh.edu.cn; shan87@xjtu.edu.cn; houyuzhu@xjtu.edu.cn

effects and profoundly affects the prognosis of cancer treatment. IR upregulates type I IFN expression, thereby inducing programmed death ligand 1 (PD-L1) expression on myeloid cells, both dampen the antitumor response[9–11]. Moreover, some subsets of neutrophils, monocytes, macrophages, and Tregs are enhanced following local tumor radiation[12]. These cells mediate tumor radioresistance by promoting immunosuppression and interfering with T-cell activation[13,14]. Exploring an efficient strategy that could overcome IR-induced "protumor" effects is necessary to amplify the antitumor immune response during RT and enhance curability.

Monocytes and macrophages are major components of the tumor microenvironment and account for up to 50% of solid tumors[15,16]. Previous studies have shown that CD11b$^+$Ly6C^{high} myeloid cells are increased in irradiated tumors and that some subsets are protumorigenic due to their immunosuppressive effects on CD8$^+$ T cells[12,14,17]. Considering that CD8$^+$ T cells play a critical role in the radiation-induced antitumor response, reducing protumorigenic cells and attenuating their immunosuppression specifically are essential goals. Combining immune checkpoint blockade with RT has been confirmed to result in better control of tumors in mouse models and patients[18,19]. This finding illustrates that strengthening CD8$^+$ T-cell function by thwarting the immunosuppressive response can potentially prevent radioresistance.

In the present study, we report that radiation enhances CXCL13 expression, which promotes CXCR5$^+$ monocytes infiltration. CXCR5$^+$ monocytes, as an immunosuppressive factor, are induced by tumor-derived VEGF and have the potential to differentiate into CXCR5$^+$ macrophages with M2 features. Inhibiting the infiltration, function, or differentiation of CXCR5$^+$ monocytes restores T-cell function and enhances tumor control during radiation. These results reveal the mechanism of radiotherapy-induced protumor effects and provide a novel direction for therapeutic strategies to overcome radioresistance.

Results

CXCL13 and CXCR5$^+$ monocytes increased in the tumor microenvironment after IR

Emerging evidence has shown that tumor infiltration of monocytes may account for therapy resistance. To determine the impact of radiation on the tumor immune microenvironment, we examined tumor immune cells at the early phase, revealing a significant increase of monocytes (Ly6C^{high}Ly6G^{low}) (Supplementary Fig. 1A). We next confirmed these findings in MC38, PanC02, and 4T1 tumor models on the 3rd day and 7th day of IR. Similarly, a striking increase in the number of tumor-infiltrated monocytes was observed 3 days after irradiation (Fig. 1A–C), whereas neutrophils (Ly6G^{high}Ly6C^{low}) were not induced by radiation (Supplementary Fig. 1B). Furthermore, no remarkable differences in tumor volume or necrosis (rarely observed) between the untreated and irradiated groups at the indicated time points (Supplementary Fig. 1C and D). Bulk tumor RNA-seq revealed that *Ly6c2* was highly expressed post-IR, whereas other leukocyte antigen-6 genes did not significantly increase after radiation (Supplementary Fig. 1E, F).

Since an abundance of chemokines can be released from tumor tissues and myeloid cells can be recruited at the initial stage after IR exposure, we next scanned chemokines in tumor tissues subjected to irradiation or not. We noted that CXCL13 was increased post-IR (Fig. 1D and E), which has been reported to be an immunosuppressive mediator in chemotherapy and immune checkpoint blockade treatment. The CXCL13–CXCR5 axis facilitates tumor metastasis and is associated with poor prognosis in colorectal cancer and breast cancer patients[20–23]. However, the function of the CXCL13–CXCR5 axis in the IR-induced immune response has not been characterized in detail. Thus, we sought to determine whether CXCL13 induced monocyte infiltration following irradiation. We analyzed CD45$^+$CXCR5$^+$ subsets of tumor 3 days and 7 days after IR. CD45$^+$CXCR5$^+$ cells were significantly increased on the day 3 of IR; notably, the increased CXCR5$^+$ population was mainly monocytes. We also noted that on the day 7 post IR, CXCR5$^+$ monocytes receded, whereas the proportions of CXCR5$^+$ mono-macrophages and CXCR5$^+$ macrophages increased (Fig. 1F and G, Supplementary Fig. 1G). These results are consistent with those of RNA-seq, which revealed that the expression of myeloid cell differentiation-associated genes *Lyz2* and *Csfr1* increased after IR (Supplementary Fig. 1F).

To further characterize CXCR5$^+$ monocytes, we compared them with CXCR5$^-$ monocytes and tumor infiltrated monocytes (CD45$^+$CD11b$^+$Ly6C^{high}Ly6G^{low} in untreated tumor). Result showed that: 1) both with and without radiation, the proportion of the CX3CR1$^+$CCR2$^-$ subset was similar across tumor infiltrated monocytes, CXCR5$^-$ and CXCR5$^+$ monocytes; 2) the CX3CR1$^-$CCR2$^+$ subset accounted for a small proportion of these three cell types; and 3) CCR2$^-$CX3CR1$^-$CXCR5$^+$ monocytes were expanded in irradiated tumors (Fig. 1H). Furthermore, the proportion of CXCR5$^+$ monocytes significantly increased in myeloid cells and tumor tissues on the 3rd day of IR in MC38 tumor-bearing mice (Fig. 1I and Supplementary Fig. 2A); nevertheless, local tumor irradiation did not affect the CXCR5$^-$ monocyte population or CXCR5 expression on monocytes (Supplementary Fig. 2B–E). A similar effect was observed in the PanC02, 4T1, and LLC tumor models (Fig. 1J, 1K, and Supplementary Fig. 2F–H). Thus, the increased CXCL13 in irradiated tumors may recruit CXCR5$^+$ monocytes specifically, resulting in monocyte expansion.

Tumor-derived VEGF induced CXCR5 expression on monocytes via the PI3K/Akt/mTOR/HIF-1α pathway

These findings prompted us to further explore the source of CXCR5$^+$ monocytes. We analyzed monocytes in the PB and BM of naïve mice and tumor-bearing mice. In tumor-bearing mice, monocytes in the PB and BM expanded at 15 days post tumor inoculation (Supplementary Fig. 3A). Moreover, there was a significant expansion of CXCR5$^+$ monocytes but not of CXCR5$^-$ monocytes in the PB and BM of tumor-bearing mice (Supplementary Fig. 3B). Compared with that in naïve mice, CXCR5 expression on monocytes from PBs (Fig. 2A) and BMs (Fig. 2B) was increased in tumor-bearing mice regardless of ionizing radiation. We next validated our findings via the use of BM-derived monocytes in vitro. CXCR5 expression increased in monocytes cultured with MC38 cells (Fig. 2C). Given that CXCR5$^+$ monocytes expanded in the PB and BM of tumor-bearing mice and that tumor cells can induce CXCR5 expression on monocytes, we postulated that tumors may upregulate CXCR5 expression on monocytes remotely. To address this hypothesis, we separated the supernatants of the tumor cells and filtered the cell components with a 0.44 μM filter. The monocytes supplemented with tumor supernatant (TS) highly expressed CXCR5 (Fig. 2C). The same results were observed for monocytes treated with TS from various tumor cell lines (Supplementary Fig. 3C and D) and for monocytes from PB and BM (Supplementary Fig. 3E). In addition, TS-induced CXCR5 expression occurred in a dose- (Supplementary Fig. 3F) and time-dependent (Supplementary Fig. 3G) manner. In the MC38 tumor model, CXCR5 expression increased in PBMCs (Supplementary Fig. 3H) and tumor-infiltrated monocytes (Supplementary Fig. 3I) with increasing inoculation time. These results suggest that tumors are necessary for the induction of CXCR5$^+$ monocytes.

We next sought to uncover how tumors induce CXCR5 expression on monocytes. Wnt signaling and NF-κB signaling were reported to be responsible for CXCR5 expression on immune cell[24–26] and tumor cells[27]. However, an NF-κB inhibitor (BAY 11-7082) or a Wnt/β-catenin inhibitor (salinomycin) did not reduce TS-induced CXCR5 expression on monocytes (Supplementary Fig. 4A). Notably, differentially expressed genes in of CXCR5$^+$ and CXCR5$^-$ monocytes were enriched in PI3K-Akt signaling (Fig. 2D). Furthermore, inhibiting PI3K with LY294002 rescued highly expressed CXCR5 in TS-treated monocytes

https://doi.org/10.1038/s41467-026-70858-6

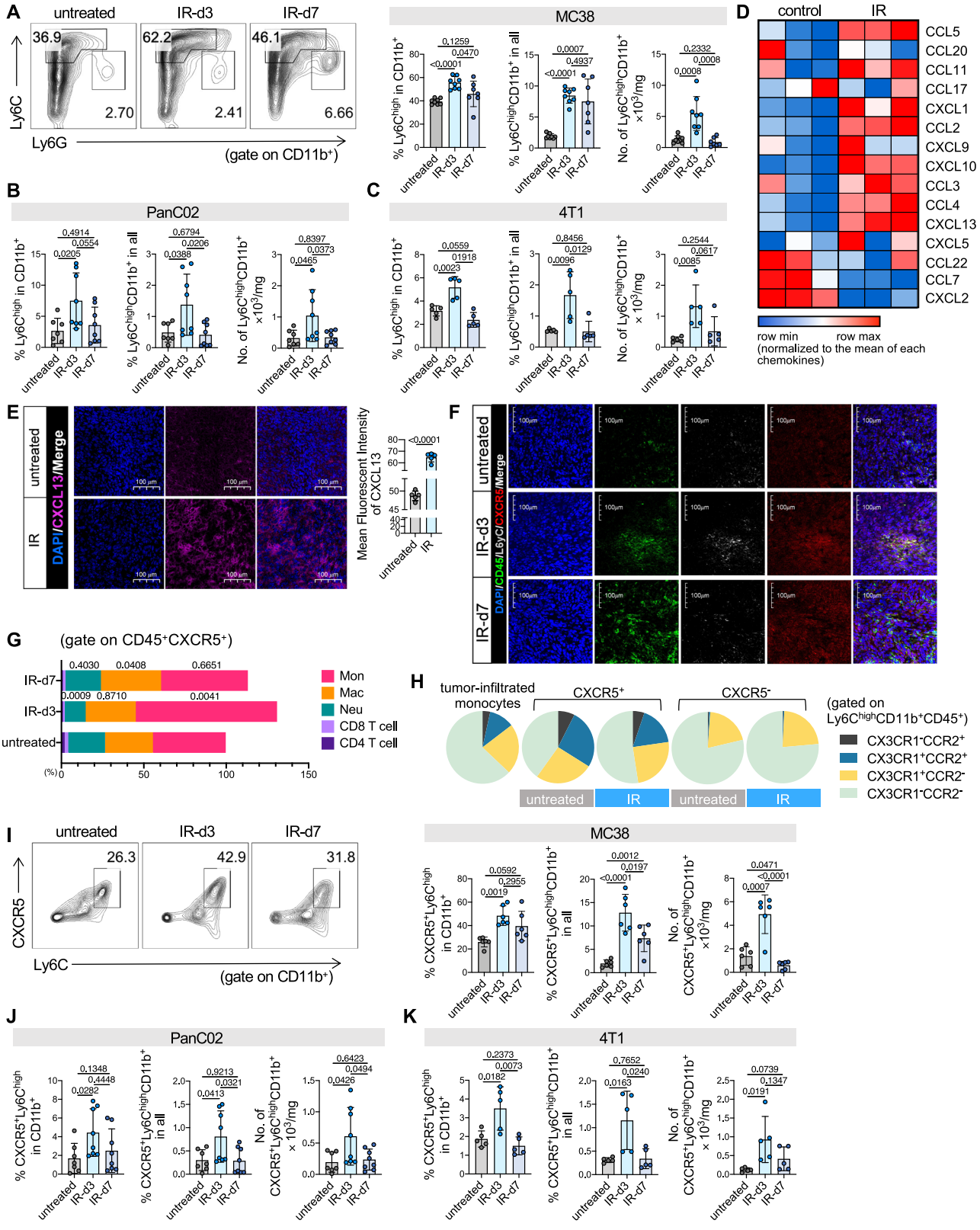

(Fig. 2E). Our results are consistent with those of a previous report indicating that PI3K activation mediates CXCR5 expression on Tfh cells[28]. The PI3K/Akt/mTOR (PAM) signaling pathway is a highly conserved signal transduction network which involved in M1/M2 polarization, anti-inflammatory effects, and polymorphonuclear neutrophil chemotaxis[29–33]. Here, we used rapamycin, an mTORC1 inhibitor, to confirm whether the PAM regulates CXCR5 expression in monocytes. We observed a decrease in the CXCR5⁺ population in rapamycin-pretreated monocytes after TS treatment (Fig. 2F). mTOR has been reported to regulate various transcription factors[34–36], among which *Eif4g2*, *Hif1a*, and *Maf* are highly expressed in CXCR5⁺ monocytes (Supplementary Fig. 4B). We constructed eIF4G2-, HIF1a-, and Maf-knockdown monocytes with siRNA (Supplementary Fig. 4C–E). With TS treatment, HIF1a-knockdown monocytes expressed less CXCR5

Fig. 1 | Radiation promoted CXCL13 expression and enhanced CXCR5$^+$ monocytes infiltration in tumor. A–C The proportion and cell number of monocytes in MC38 (**A**), PanC02 (B), and 4T1 (**C**) tumors. Tumors received one dose of 12 Gy ironizing radiation (IR) 10 days post tumor inoculation and were removed three or seven days after IR. Cell suspension was analyzed by flow cytometry. For MC38 tumor models, $n = 8$ in untreated and IR-d3 groups, $n = 7$ in IR-d7 group. For PanC02 tumor models, $n = 7$ in untreated groups, $n = 8$ in other groups. $n = 5$ mice/group for 4T1 tumor model. **D** The quantitation of chemokines in tumor with or without radiation. $n = 3$ biological replicates. **E** Mean fluorescence intensity staining of tumor tissue. CXCL13 (magenta), nuclear (blue). $n = 5$ mice/group. **F** Immunofluorescence staining of tumor tissue. CD45 (green), Ly6C (gray), CXCR5 (red), nuclear (blue). Data is representative of $n = 3$ biological replicates. **G** The components of CXCR5$^+$ population in tumor. $n = 5$ mice/group. **H** The expression of CCR2 and CX3CR1 on tumor infiltrated monocytes. $n = 6$ mice/group. **I–K** The proportion and quantity of CXCR5$^+$ monocytes in MC38 (**I**), PanC02 (**J**), and 4T1 (**K**) tumors. For MC38 tumor models, $n = 7$ mice/group. For PanC02 tumor models, $n = 7$ in untreated groups, $n = 8$ in other groups. $n = 5$ mice/group for 4T1 tumor model. Statistical analysis by two-sided unpaired t-test (**D**, **E**) or one-way analysis of variance (ANOVA) (**A–C**, **G**, and **I–K**). Data are represented as mean ± SD (**A–C**, **G**, and **I–K**); * $p < 0.05$; ** $p < 0.01$; *** $p < 0.001$ and NS, not significant.

(Fig. 2G), while WT monocytes highly expressed HIF-1α (Fig. 2H). Taken together, these findings indicate that tumors can release certain soluble substances to induce monocyte CXCR5 expression, which is PI3K/Akt/mTOR/HIF-1α dependent.

To further explore which soluble substances in tumors induce CXCR5 expression on monocytes via PAM, we cultured monocytes with TS filtered through membranes with different pore sizes or with inhibited tumor exosomes, and the results revealed that CXCR5 expression was not affected by insoluble factors, including extracellular vesicles (Supplementary Fig. 4F and G). Previous studies reported that tumor cells can generate prostaglandin E2 (PGE_2)[37] and induces CXCR5 expression on THP-1 cells[26]. Therefore, we applied PGE_2 to monocytes as described in previous studies[26]. Although 20 ng/ml PGE_2 enhanced CXCR5 expression (Supplementary Fig. 4H), inhibiting cyclooxygenase-2 (a key synthetase of PGE_2) in MC38 or monocytes (Supplementary Fig. 4I) or knocking out *Ptgs2* in the MC38 tumor cell line (Supplementary Fig. 4J) did not rescue the upregulation of CXCR5 in TS-treated monocytes. These results suggest that PGE2 is not the main mediator of CXCR5 expression in monocytes under tumor conditions.

Tumor-derived small molecules or soluble proteins have been verified to mediate myelopoiesis and enhance tumor-promoting properties[38], we next focused on the tumor-derived soluble immunosuppressive factors thromboxane A2 (TXA_2), indoleamine 2,3-dioxigenase (IDO), adenosine, TGF-β, EGF, and VEGF[39–42]. We treated monocytes with receptor antagonists or inhibitors of these factors before culture with TS. The results showed that inhibiting TGF-β, EGF, and VEGF rescued TS-induced CXCR5 expression (Fig. 2I). Moreover, recombinant murine (rm) VEGF and EGF enhanced CXCR5 expression on monocytes (Fig. 2J). Compared with WT-TS-induced CXCR5, *Vegfa* knock out (KO)-TS and *Egf* KO-TS weakened CXCR5 expression on monocytes (Fig. 2K). In addition, anti-VEGF-A reversed TS-induced CXCR5 expression (Fig. 2L). We also found that rmVEGF was activated in monocytes (Fig. 2M) and that a VEGFR inhibitor impaired TS-induced PAM signaling activation (Fig. 2N). In naïve mice, rmVEGF enhanced CXCR5 expression on monocytes in BM and PB (Fig. 2O). Anti-VEGF-A reduced CXCR5 expression on monocytes in tumor-bearing mice (Fig. 2O). *Vegfa*-KO MC38 inoculation and regorafenib treatment inhibited CXCR5 expression on monocytes in the tumor, PB, and BM of tumor-bearing mice (Fig. 2P and Q). Furthermore, regorafenib reduced the proportion of monocytes in PBs and tumors (Fig. 2R). These findings establish that tumors release VEGF and induce CXCR5 expression on monocytes. The expanded CXCR5$^+$ monocytes served as a "reserve pool" and were prepared for radiation-induced monocyte infiltration.

IR promoted the tumoral infiltration of CXCR5$^+$ monocytes through the CXCR5–CXCL13 axis

Since numerous chemokines are upregulated in tumor tissues after IR (Fig. 1D), we investigated which of these contribute to monocyte recruitment using selective antagonists and neutralizing antibodies. Blockade of CXCL13 signaling, but not CCL4, CCL5, CXCL1, and CXCL10 signaling, abrogated radiation-induced monocyte infiltration (Fig. 3A and Supplementary Fig. 5A), which suggested that CXCL13-CXCR5 axis is more important for monocyte recruitment in irradiated tumor.

In the IR condition, we observed a significant increase of the percentage and number of monocytes (Fig. 3B), especially CXCR5$^+$ monocytes, in the PB (Fig. 3C), which is consistent with the findings in tumor tissues. To further investigate whether increased CXCL13 levels accelerated CXCR5$^+$ monocyte migration and tumor infiltration, we performed an ex vivo transwell assay. Homogenates of tumor tissues from untreated or IR-treated mice were added to the lower chambers. TS-treated WT or CXCR5$^{-/-}$ monocytes were added to the upper chambers. After 4 h of culture, the cells in the lower chamber were collected and analyzed via flow cytometry (Fig. 3D). We found that compared with untreated tumors, IR-treated tumors recruited more WT monocytes but fewer CXCR5$^{-/-}$ monocytes in irradiated tumors (Fig. 3E and Supplementary Fig. 5B). In accordance with the results ex vivo, monocytes increased in the tumors of WT mice post-IR but decreased in those of CXCR5$^{-/-}$ (Fig. 3F), anti-VEGF-A treated (Fig. 3G), and *Vegfa*-KO tumor-bearing mice (Fig. 3H). These data suggested that IR recruited monocytes via CXCR5 on monocytes. To further verify whether irradiated tumors recruit CXCR5$^+$ monocytes via enhanced CXCL13, we next added a CXCL13-neutralizing antibody to the homogenate of IR-treated tumors (Fig. 3I). The results showed that neutralizing CXCL13 reduced radiation-induced CXCR5$^+$ monocyte migration (Fig. 3J). In tumor-bearing mice, CXCL13 neutralization significantly weakened the infiltration of CXCR5$^+$ monocytes and monocytes post-IR (Fig. 3K). However, CXCL13 neutralization did not affect CXCR5$^-$ monocyte infiltration (Supplementary Fig. 5C). These findings demonstrated that by inducing CXCL13 production, local tumor radiation recruited monocytes, most of which were CXCR5$^+$ cells.

To determine the source of CXCL13 after IR, we analyzed IR-treated tumors and found that the proportion of CXCL13$^+$ cells increased (Fig. 3L and Supplementary Fig. 5D), among which CD45$^-$ cells strikingly expanded post-IR (Fig. 3M). Hence, we hypothesized that tumor cells are the main source of CXCL13 during radiation. We then delivered radiation to the tumor cells directly. Interestingly, the level of CXCL13 increased slightly in tumor cells after IR. Tumor cells cultured with macrophages also showed mild upregulation of CXCL13. Notably, IR-treated tumor cells cultured with macrophages (with or without IR) highly expressed CXCL13 (Fig. 3N). We concluded that macrophages were necessary for tumor cells to produce CXCL13 following IR. We also found that, in *Cxcl13* KO MC38 tumor-bearing mice and macrophage-deficient mice, IR did not significantly enhance CXCL13 in tumor tissues (Supplementary Fig. 5E). Moreover, monocytes, especially CXCR5$^+$ monocytes, were reduced in the PB and tumor tissue after local irradiation (Fig. 3O and Supplementary Fig. 5F). Blocking the CXCL13–CXCR5 axis (CXCR5 deficiency in monocytes or CXCL13 reduction in tumors) decreased monocyte and CXCR5$^+$ monocyte infiltration after IR. Taken together, our data indicate that radiation, as a stimulus, increases CXCL13 in tumor cells, thereby prompting CXCR5$^+$ monocytes to migrate from the "reserve pool" to the tumor tissue.

https://doi.org/10.1038/s41467-026-70858-6

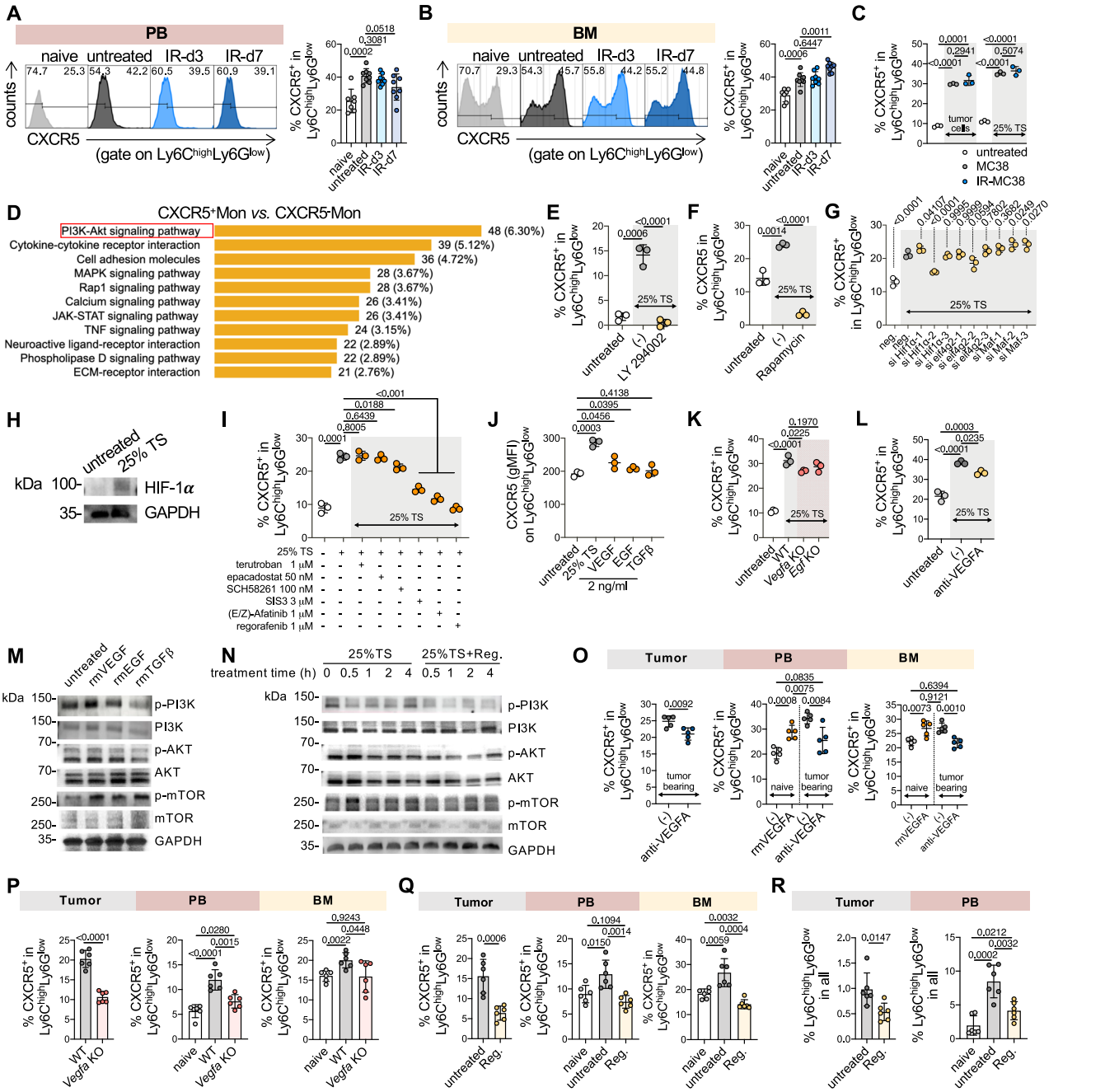

Fig. 2 | Tumor derived VEGF induced CXCR5 expression on monocytes through PI3K/Akt/mTOR/HIF-1α pathway. A, **B** CXCR5 expression on monocytes from peripheral blood (PB) (**A**) and bone marrow (BM) (**B**). IR, ironizing radiation. $n = 7$ in naive groups, $n = 8$ in other groups. **C** CXCR5 expression on monocytes cultured with tumor cell or tumor supernatant (TS). **D** KEGG pathway analysis of differentially expressed genes of $CXCR5^+$ monocytes and $CXCR5^-$ monocytes. **E**–**G** CXCR5 expression on monocytes. 10 μM LY294002 (PI3K inhibitor) (**E**) and 10 μM rapamycin (mTOR inhibitor) (**F**) pretreated or Hif-1α-, eif4g-, and Maf-knock down (**G**) monocytes were cultured with 25% TS and analyzed. **H** Immuno-blotting analysis of HIF-1α in 25% TS treated monocytes. **I** CXCR5 expression on monocytes. Terutroban, epacadostat, SCH58261, SIS3, (E/Z)-Afatinib and regorafenib pretreated monocytes were cultured with 25% TS and analyzed. **J**–**L** CXCR5 expression on monocytes. Monocytes cultured with cytokines (**J**), 25% TS from indicated cells (**K**), or 2 μg/ml anti-VEGF pretreated TS (**L**) were analyzed. **M**, **N** Immuno-blotting analysis of indicated phosphorylated (p-) and total protein in monocytes cultured with rmVEGF, EGF and TGFβ for 2 h (M) or monocytes pretreated with or without regorafenib for 30 min and then cultured with TS for indicated time (**N**). **O**, **P** CXCR5 expression on monocytes of PB, BM and tumor. All samples were collected and analyzed on 15 days after tumor inoculation. Treatment details are provided in method. $n = 5$ mice/group (**O**). $n = 6$ mice/group (**P**). **Q**, **R** CXCR5 expression on monocytes (**T**) and the proportion of monocytes (**U**) of PB, BM and tumor from naïve mice, tumor bearing mice and regorafenib-treated mice. Mice were treated with 10 mg/kg regorafenib, orally, every day from 7 days after tumor inoculation. $n = 6$ mice/group. $n = 3$ cells examined over 2 independent experiments (**C**, **E**–**N**). Statistical analysis by two-sided unpaired t-test (**O**–**R**) or one-way ANOVA (**A**–**C**, **E**–**G**, **I**–**L**, **O**–**R**). Data are represented as mean ± SD; * $p < 0.05$; ** $p < 0.01$; *** $p < 0.001$ and NS, not significant.

https://doi.org/10.1038/s41467-026-70858-6

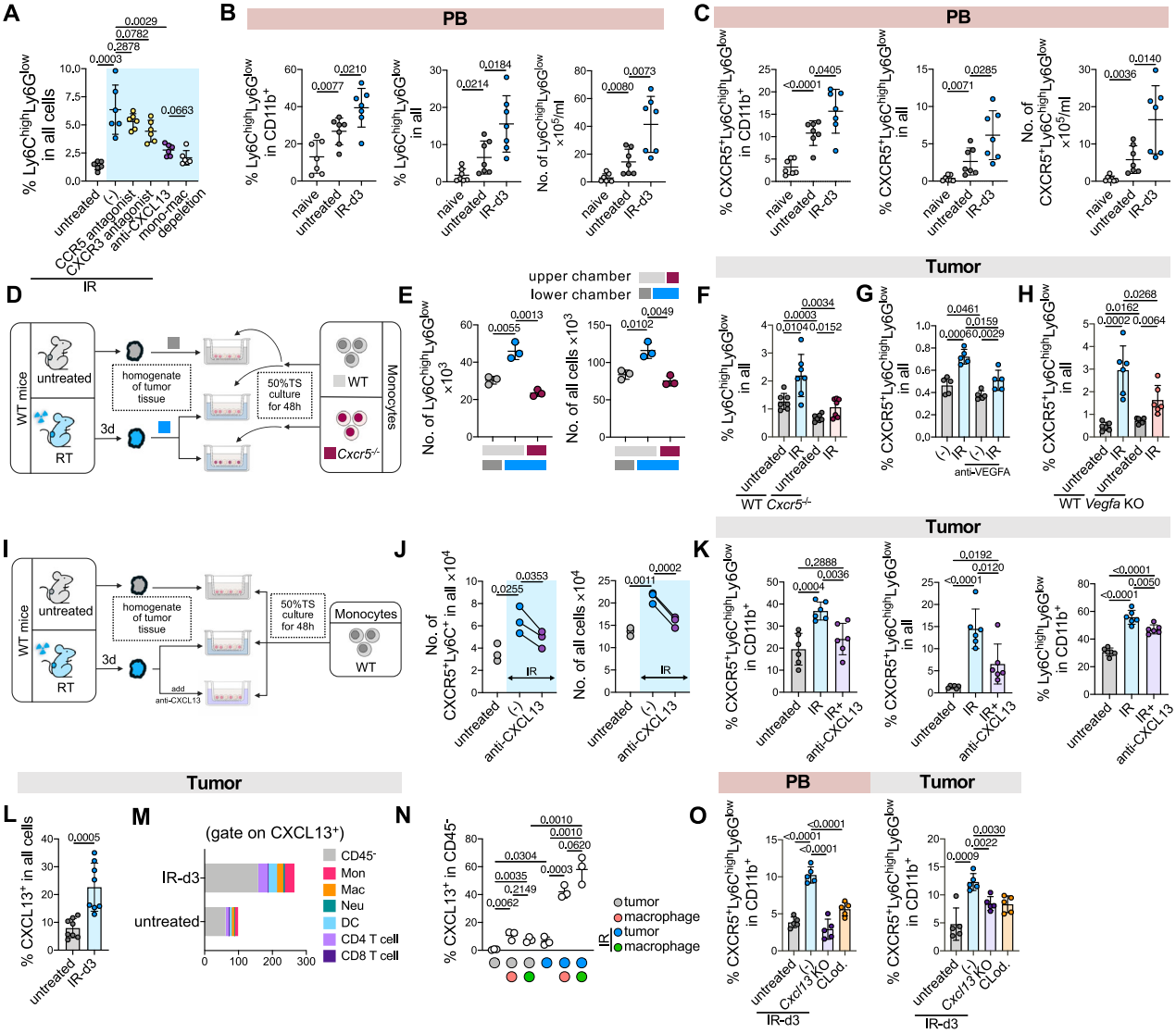

Fig. 3 | Radiation recruited CXCR5⁺ monocytes into tumor microenvironment through CXCR5/CXCL13 axis. A Monocytes in irradiated tumors. Tumor-bearing mice were treated with CCR5 antagonist, CXCR3 antagonist, anti-CXCL13, and anti-CSF1R at the day of ironizing radiation (IR). Tumors were separated and analyzed 3 days post IR. $n = 6$ mice/group. **B**, **C** The proportion of monocytes (**B**) and CXCR5⁺ monocytes (**C**) in PB. $n = 7$ mice/group. **D** Schematic diagram of monocytes trans-well assay. Created with MedPeer (medpeer.cn). **E** The quantity of migrated monocytes. **F** The proportion of monocytes in tumor. $n = 7$ mice/group. **G**, **H** CXCR5⁺ monocytes in tumor. $n = 5$ mice/group (**F**). $n = 6$ mice/group (**G**). **I** Schematic diagram of monocytes trans-well assay. Created with MedPeer (medpeer.cn). **J** The quantity of migrated monocytes. **K** The proportion and quantity of monocytes and CXCR5⁺ monocytes in irradiated tumor with or without anti-CXCL13 treatment. $n = 6$ mice/group. **L** The proportion of CXCL13⁺ cells in tumor. $n = 8$ mice/group. **M** The relative quantity of CXCL13⁺ cells and its components in tumor tissue. $n = 5$ mice/group. **N** The proportion of CXCL13⁺ tumor cells with or without IR treatment, and in the present with macrophages or not. **O** The proportion of CXCR5⁺ monocytes in PB and tumor of *Cxcl13*-KO group and clodronate liposomes (Clod.) treatment group. Clod. was administered intraperitoneally, 1 mg/mouse, every other day from 3 days before radiation. $n = 5$ mice/group. $n = 3$ cells examined over 2 independent experiments (**E**, **J**, and **N**). Statistical analysis by two-sided one-way ANOVA (**A**–**C**, **E**–**H**, **J**, **K**, **N** and **O**), unpaired t-test (**J**–**L**) or paired t-test (**J**). Adjustments were made for multiple comparisons. Data are represented as mean ± SD; * $p < 0.05$; ** $p < 0.01$; *** $p < 0.001$ and NS, not significant.

Reducing tumor-infiltrating CXCR5⁺ monocytes enhanced CD8⁺ T-cell-dependent antitumor immunity

We next sought to determine whether and how CXCR5⁺ monocytes affect the efficacy of RT. Tumor-bearing mice were adoptively transferred with CXCR5⁻ and CXCR5⁺ monocytes from the day of irradiation. The tumor growth revealed that CXCR5⁺ monocytes had an impaired therapeutic effect, whereas CXCR5⁻ monocytes did not (Fig. 4A). We then employed CXCR5⁻/⁻ tumor-bearing mice and administered IR. Compared with WT mice, CXCR5⁻/⁻ mice presented pronounced inhibition of tumor growth (Fig. 4B). *Vegfa*-KO tumors presented better control following IR than did WT tumors (Fig. 4C). Furthermore, CXCL13 deficiency in tumor cells (Fig. 4D) and CXCL13 neutralization in irradiated tumors (Fig. 4E) enhanced tumor control and prolonged the survival of tumor-bearing mice after radiation (Fig. 4F). These data suggested that CXCR5⁺ monocytes weakened tumor control after IR treatment.

To understand how CXCR5⁺ monocytes impair IR efficiency, we conducted rechallenge models using tumor-rejected mice in the IR and anti-CXCL13 combination groups (Fig. 4G). In naïve mice, the tumor volume of MC38 cells increased progressively. Conversely, MC38 was completely inhibited in tumor-rejected mice (Fig. 4H). The LLC tumors grew normally in these two groups (Fig. 4I). These results suggested that CXCR5⁺ monocytes weakened adaptive immunity. We then depleted CD8⁺ T cells in mice and observed that neutralizing CXCL13

https://doi.org/10.1038/s41467-026-70858-6

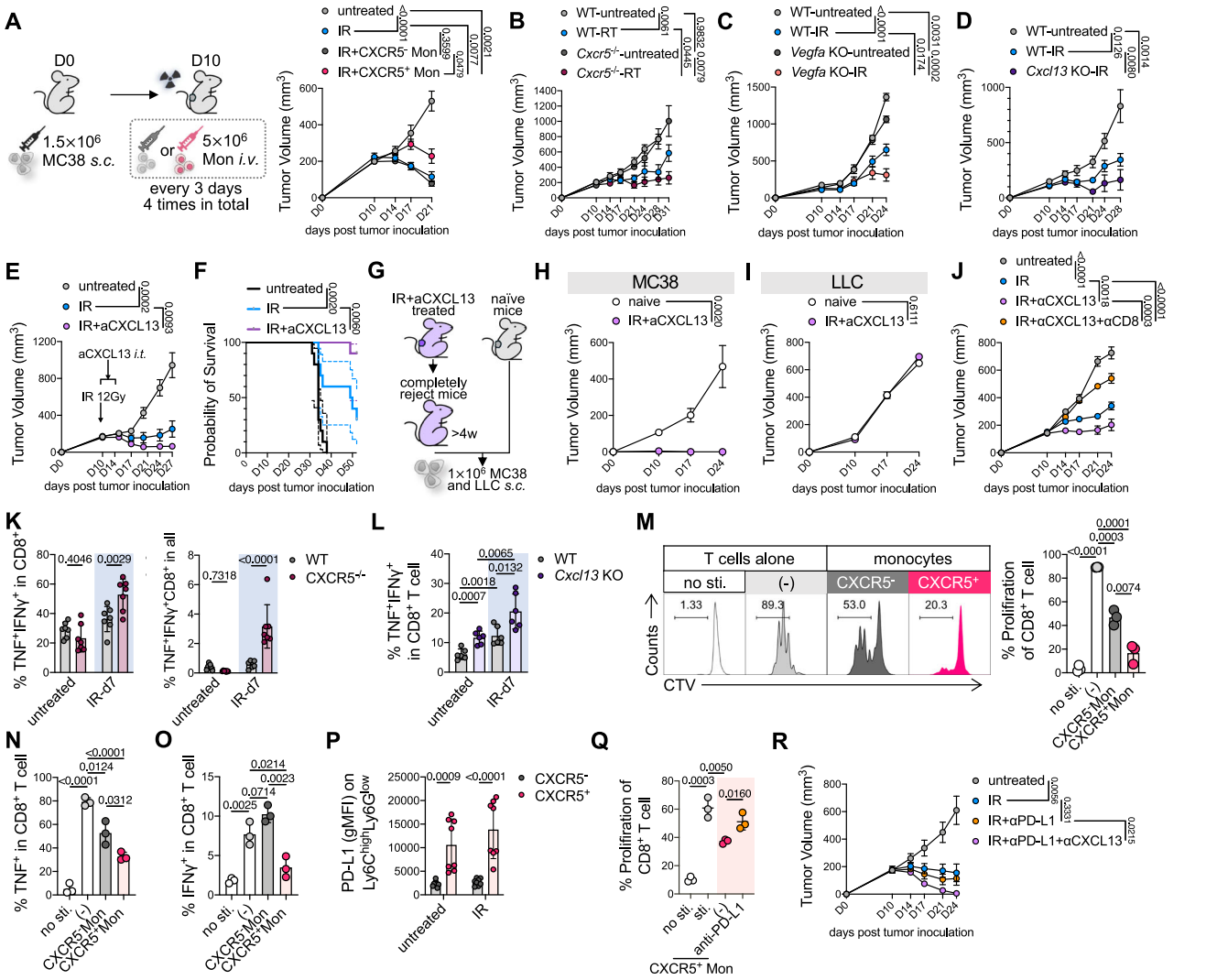

Fig. 4 | CXCR5⁺ monocytes inhibited radiation-induced antitumor immune responses. A Tumor growth of mice treated with monocytes intravenously transfer and tumor radiation. Details are provided in method. IR, ironizing radiation. $n = 5$ mice/group. **B**–**D** Tumor growth of WT and *Cxcr5*$^{-/-}$ mice (**B**), *Vegfa*-KO (**C**) and *Cxcl13*-KO (**D**) MC38 tumor. $n = 5$ mice/group. Tumor growth (**E**) and survival (F) of MC38 tumor–bearing mice treated with IR and CXCL13 neutralization. $n = 10$ mice/group. **G** Schematic diagram of rechallenge model. (H and I) Tumor growth of MC38 (**H**) and LLC (**I**) tumors following reinoculation. $n = 5$ mice/group. **J** Tumor growth of CD8⁺ T cells depleting mice treated with IR and anti-CXCL13. $n = 5$ mice/group. **K**, **L** The proportion of TNF⁺IFNγ⁺CD8⁺ T cells in tumors of WT and *Cxcr5*$^{-/-}$ mice (**K**), WT and *Cxcl13*-KO MC38 tumor (**L**). $n = 7$ mice/group (**K**). $n = 6$ mice/group (**L**). **M**–**O** T cell activation assay. **P** PD-L1 expression on tumor infiltrated CXCR5⁺ monocytes. $n = 8$ mice/group. **Q** T cell proliferation in the presence of CXCR5⁺ monocytes with or without anti-PD-L1. **R** Tumor growth of mice treated with IR, CXCL13 neutralization, and anti-PD-L1. $n = 5$ mice/group. $n = 3$ cells examined over 2 independent experiments (**M**–**O** and **Q**). Statistical analysis by two-way ANOVA (**A**–**E**, **H**–**L**, and **R**), two-sided log rank (Mantel-Cox) test (**F**), or one-way ANOVA (**M**–**Q**). Data shown in panels (**A**–**J**, **R**) are represented as mean ± SEM, other panels are represented as mean ± SD; * $p < 0.05$; ** $p < 0.01$; *** $p < 0.001$, and NS, not significant.

after IR did not enhance antitumor efficiency (Fig. 4J). Thus, we hypothesized that CXCR5⁺ monocytes impaired the CD8⁺ T-cell response after radiation. In accordance with the enhanced efficiency, IR induced greater expression of TNF and IFNγ in tumor-infiltrating CD8⁺ T cells from CXCR5$^{-/-}$ mice (Fig. 4K) and *Cxcl13* KO tumors (Fig. 4L) than in those from control mice. Furthermore, host CXCR5 deficiency or neutralization CXCL13 after radiation augmented total and activated CD8⁺ T cells in tumor tissues (Supplementary Fig. 6A–C). To determine whether CXCR5⁺ monocytes have direct effects on T cells, we conducted a T-cell activation assay and observed that, compared with CXCR5⁻ monocytes, CXCR5⁺ monocytes more strongly inhibited the proliferation and expression of TNF and IFNγ in CD8⁺ T cells (Fig. 4M–O). Consistent effects were observed in CD4⁺ T cells (Supplementary Fig. 6D–F). These results demonstrated that CXCR5⁺ monocytes have increased immunosuppressive activity and could impair the efficacy of radiation by inhibiting CD8⁺ T-cell function.

Next, we identified the genes expressed in CXCR5⁺, CXCR5⁻ monocytes from irradiated tumors and monocytes from untreated tumors to investigate how CXCR5⁺ monocytes attenuate CD8⁺ T-cell function. The results revealed that CXCR5⁺ monocytes demonstrate an enhanced expression of protumor genes, including *Arg1*, *Hif1a*, and *Spp1*, when compared with either tumor inflitrated monocytes or CXCR5⁻ monocytes. In contrast, CXCR5⁺ monocytes exhibited an attenuated antitumor gene profile, including IL12a, CD86, and ICOSL (Supplementary Fig. 6G). In accordance with the gene expression profiles of CXCR5$^{-/+}$ monocytes, PD-L1 highly expressed in tumor-infiltrated CXCR5⁺ monocytes in MC38, PanC02, and 4T1 tumor-bearing mice (Fig. 4P, Supplementary Fig. 6H and I). In TS-treated

monocytes, PD-L1 expression increased in CXCR5$^+$ monocytes (Supplementary Fig. 6J). We next investigated whether PD-L1/PD-1 signaling mediated CXCR5$^+$ monocyte-induced CD8$^+$ T-cell inhibition. CXCR5$^+$ monocytes pretreated with or without anti-PD-L1 were cultured with activated T cells. The result showed that anti-PD-L1 reversed the CXCR5$^+$ monocyte-induced inhibition of CD8$^+$ and CD4$^+$ T-cell proliferation (Fig. 4Q and Supplementary Fig. 6K). Furthermore, RT combined with anti-PD-L1 and anti-CXCL13 significantly improved tumor control (Fig. 4R). On the basis of this observation, we surmised that reducing CXCR5$^+$ monocyte infiltration and blocking immune regulatory signals enhanced the effect of RT.

CXCR5$^+$ monocytes differentiated into CXCR5$^+$ macrophages

The results revealed that CXCR5$^+$ monocytes did not increase consistently after IR; nevertheless, the proportion of CXCR5$^+$ macrophages increased (Figs. 1G and 5A). Considering that monocytes can migrate to tumors and differentiate into macrophages, we hypothesized that CXCR5$^+$ monocytes may convert to CXCR5$^+$ macrophages in irradiated tumors. To test this hypothesis, we inhibited CXCR5 expression on monocytes and neutralized CXCL13 in tumors after IR, revealing that the proportion of CXCR5$^+$ macrophages decreased after radiation (Fig. 5B, Supplementary Fig. 7A and B). We next investigated how CXCR5$^+$ monocytes convert to CXCR5$^+$ macrophages after irradiation and revealing that that granulocyte–macrophage colony-stimulating factor (GM-CSF), which can promote hemopoietic stem cell differentiation, increased after radiation (Fig. 5C). In addition, the possibility that tumors induce macrophages expressing CXCR5 directly cannot be excluded. Hence, we performed two processes in vitro. In process 1, macrophages were induced with GM-CSF and treated with TS. In process 2, monocytes were treated with TS and differentiated into macrophages under GM-CSF conditions. The results revealed that TS cannot increase CXCR5 expression on macrophages and that CXCR5$^+$ macrophages are derived from CXCR5$^+$ monocytes (Fig. 5D). Furthermore, iPI3K inhibited CXCR5 expression in monocytes but did not affect macrophages (Supplementary Fig. 7C). By transferring CXCR5$^+$ monocytes (CD45.1.2) into CD45.2 mice and delivering radiation to their tumors, we verified the differentiation of CXCR5$^+$ monocytes in vivo (Fig. 5E). The results revealed that most adoptive CXCR5$^+$ monocytes polarized into macrophages in irradiated tumors, which persistently expressed CXCR5 and highly expressed CD206 (Fig. 5F). These data indicate that the increased proportion of CXCR5$^+$ macrophages following irradiation is derived mainly from CXCR5$^+$ monocytes.

M2 macrophages exhibit immunosuppressive features in the tumor[43]. We suspected that the CXCR5$^+$ macrophages derived from CXCR5$^+$ monocytes were M2-like macrophages with immunosuppressive effects. To test this, TS-induced CXCR5$^+$ monocytes were labeled with APC-Cy7 and then cultured with GM-CSF for 72 h. The results revealed that the APC-Cy7$^+$ population contained more CD206$^+$MHC II$^-$ macrophages than the APC-Cy7$^-$ population (Fig. 5G). We also found that CXCR5$^+$ macrophages expressed higher levels of CD206 after irradiation, consistent with the in vitro results (Fig. 5H). Moreover, the proportion of M2 macrophages increased in the tumor 7 days after irradiation (Fig. 5I), the same trend as that observed with CXCR5$^+$ macrophages (Fig. 5A). Blockade of the CXCR5–CXCL13 axis reversed the increase in M2-like macrophages after IR (Fig. 5J, K, and Supplementary Fig. 7D). Moreover, neutralizing IR-induced GM-CSF decreased the M2-like macrophage population but enhanced M1-like macrophages (Fig. 5L and Supplementary Fig. 7E). We analyzed the gene expression of CXCR5$^{+/-}$ monocytes and observed that CXCR5$^+$ monocytes expressed higher *Hif1a* and *Arg1* but lower *Citta* (Supplementary Fig. 7F). DEGs in CXCR5$^{-/+}$ monocytes were enriched in the PPAR signaling pathway, which regulates M2 polarization (Supplementary Fig. 7G). These results suggested that IR induced CXCR5$^+$ M2-like macrophages and that their characteristics were determined at the monocyte stage.

To further characterize CXCR5$^+$ macrophages in detail, we analyzed gene expression differences between CXCR5$^-$ and CXCR5$^+$ macrophages across functional modules. Antigen presentation- and cell cycle-associated genes were expressed at lower levels in CXCR5$^+$ macrophages than in CXCR5$^-$ cells (Supplementary Fig. 8A). Conversely, the expression of immunosuppressive genes, such as *Cd274*, *Arg1*, *Ctla2b, Mrc1*, and *Ms4a4a*, was increased in CXCR5$^+$ macrophages (Supplementary Fig. 8A). Enrichment analyses revealed that CXCR5$^+$ macrophages were less enriched in myeloid leukocyte activation and the inflammatory response (Supplementary Fig. 8B). We next confirmed whether CXCR5$^+$ M2-like macrophages play an immunosuppressive role and found that CXCR5$^+$ macrophages strongly inhibited CD8$^+$ T-cell proliferation (Fig. 5M), TNF, and IFNγ (Fig. 5N). Consistent with the findings in CXCR5$^+$ monocytes, PD-L1 expression was greater in CXCR5$^+$ macrophages (Fig. 5O). A transfer assay demonstrated that CXCR5$^+$ monocytes differentiated into macrophages that highly expressed CD206 and PD-L1 (Supplementary Fig. 8C). These results demonstrate that CXCR5$^+$ monocytes differentiate into CXCR5$^+$ macrophages with an M2-like phenotype, which inhibiting CD8$^+$ T-cell immunity. In tumor-bearing mice, combination treatment with IR and anti-GM-CSF enhanced tumor control (Fig. 5P). This finding suggests that neutralizing GM-CSF is a potential strategy for promoting the efficacy of RT by interrupting CXCR5$^+$ M2-like macrophage differentiation after irradiation.

Radiation induced human CXCR5$^+$ monocyte infiltration in tumors

To verify the relevance of our findings to cancer patients, we integrated datasets from the Gene Expression Omnibus. In pancreatic cancer (PDAC) patients, the tumor of patients who received stereotactic radiosurgery (SBRT) or conventional radiotherapy (XRT) presented high expression of *Cd14*, *Cxcr5*, and *Cd274* (Fig. 6A). We performed a systematic analysis of 31 solid tumors from the TCGA database. The results demonstrated that the expression of *Cxcr5*, *Cd14*, and immunosuppressive factors was positively correlated with *Cxcl13* (Supplementary Fig. 9A). Given these observations, we sought to verify whether irradiated tumors recruit CXCR5$^+$ monocytes. Human PBMCs were treated with TS of human pancreatic and breast cancer cell lines (Fig. 6B). After 48 h of treatment, CXCR5 highly expressed in the CD14$^+$ population (Fig. 6C and Supplementary Fig. 9B). The Transwell assay showed that the supernatant from irradiated cocultured cells recruited more TS-induced PBMCs, which expressed higher levels of CXCR5 than did the supernatant from the untreated group (Fig. 6B and D). In vivo, we established a human colonic tumor model in nude mice with HCT116 cells and transferred CTV-labeled THP-1 cells, a human monocyte-like cell line that expresses high levels of CXCR5 (Supplementary Fig. 9C). The results revealed that local tumor irradiation enhanced the infiltration of CTV$^+$CXCR5$^+$ THP-1 cells (Fig. 6E).

We next evaluated monocytes in the PB and tumor responses (according to the Response Evaluation Criteria in Solid Tumors, RECIST) of cancer patients and found that monocytes significantly increased in progressive disease (PD) patients after IR (Fig. 6F and G). However, it did not change in partial response (PR) or stable disease (SD) patients (Fig. 6F and G). In addition, there was no significant change in the number of blood platelets (PLTs) in the PR, SD, or PD patients before and after irradiation (Supplementary Fig. 9D). Immunohistochemistry showed CXCL13 expression and CXCR5$^+$ monocyte infiltration in the tumors of rectal cancer patients who received radiotherapy (Fig. 6H and I). High expression of CXCR5 was associated with poor overall survival in TCGA rectum, colon, pancreatic adenocarcinoma, and breast invasive carcinoma cohorts of (Supplementary Fig. 9E).

https://doi.org/10.1038/s41467-026-70858-6

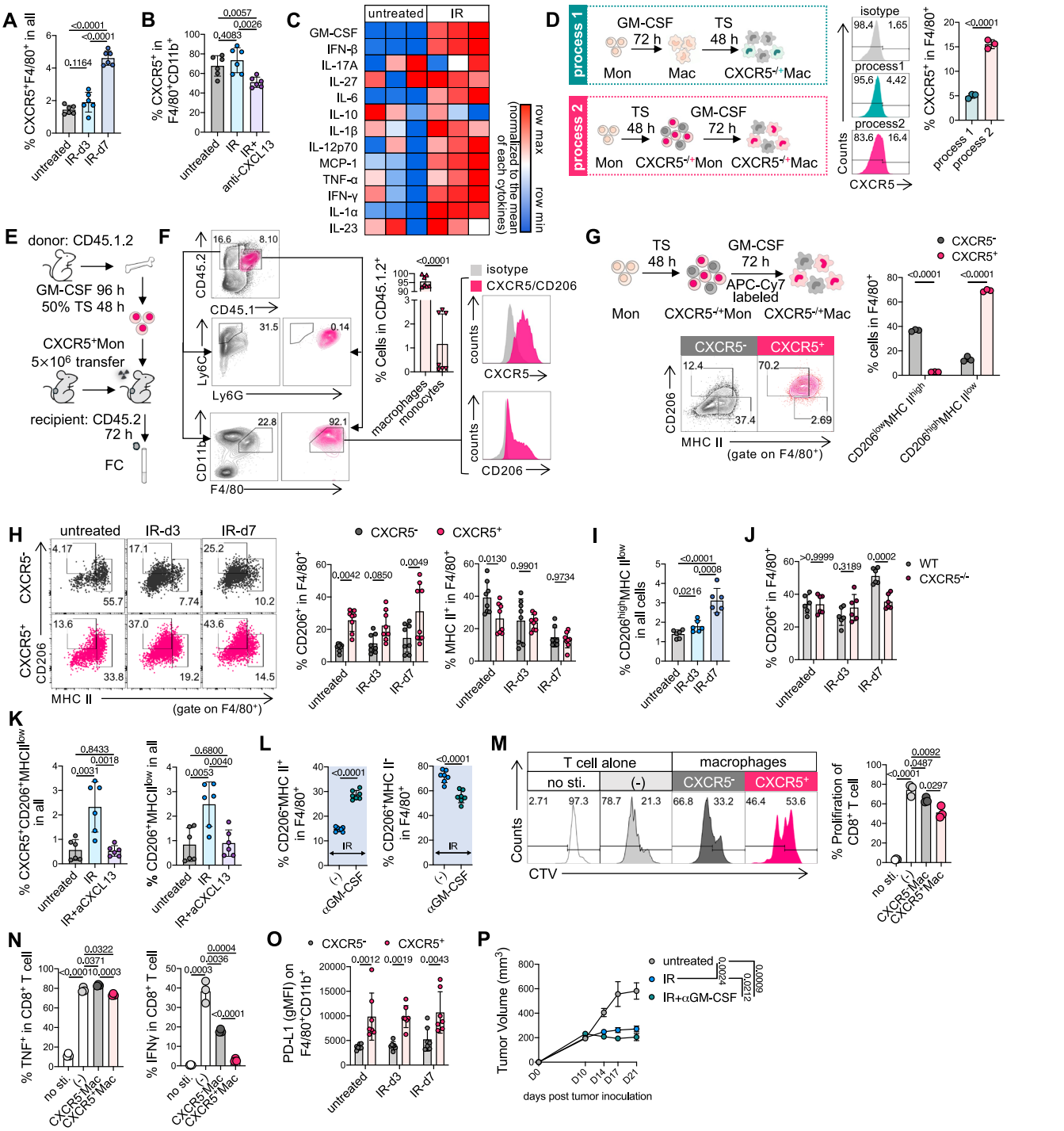

Fig. 5 | Tumor infiltrating CXCR5$^+$ monocytes differentiated towards M2-like macrophages. A, **B** The proportion of CXCR5$^+$ macrophages in tumor at day 3 (**A**) and day 7 after ironizing radiation (IR) (**A**, **B**) treated with or without anti-CXCL13 (**B**). $n = 6$ mice/group. **C** The quantitation of cytokines in tumor with or without radiation. $n = 3$ biological replicates. **D** The expression of CXCR5 on macrophages. **E** Schematic diagram of monocytes transfer assay. **F** The proportion of macrophages and monocytes in CD45.1.2$^+$ population and the expression of CXCR5 and CD206 on macrophages. $n = 7$ mice/group. **G**, **H** The proportion of M1-like and M2-like macrophages in vitro and in tumor. $n = 8$ mice/group (**H**). **I**–**K** The proportion of M2-like macrophages in tumor. Tumor of WT mice (**I**), *Cxcr5*$^{-/-}$ mice (**J**), and anti-CXCL13 treated mice (**K**) were analyzed. $n = 6$ mice/group. **L** The proportion of M1-like and M2-like macrophages in tumor treated with IR and GM-CSF neutralization. $n = 7$ mice/group. **M**, **N** T cell activation assay. **O** PD-L1 expression on CXCR5$^-$ and CXCR5$^+$ macrophages. $n = 7$ mice/group. **P** Tumor growth of mice treated with IR and GM-CSF neutralization. $n = 5$ mice/group. $n = 3$ cells examined over 2 independent experiments (**D**, **G**, **M**, **N**). Statistical analysis by two-sided one-way (**A**, **B**, **I**, **K**, **M**, and **N**) or two-way ANOVA (**G**, **H**, **J**, **O**, and **P**), or unpaired t-test (**C**, **D**, **F**, and **L**). Data shown in panel (**O**) is represented as mean ± SEM, other panels are represented as mean ± SD; * $p < 0.05$; ** $p < 0.01$; *** $p < 0.001$ and NS, not significant.

https://doi.org/10.1038/s41467-026-70858-6

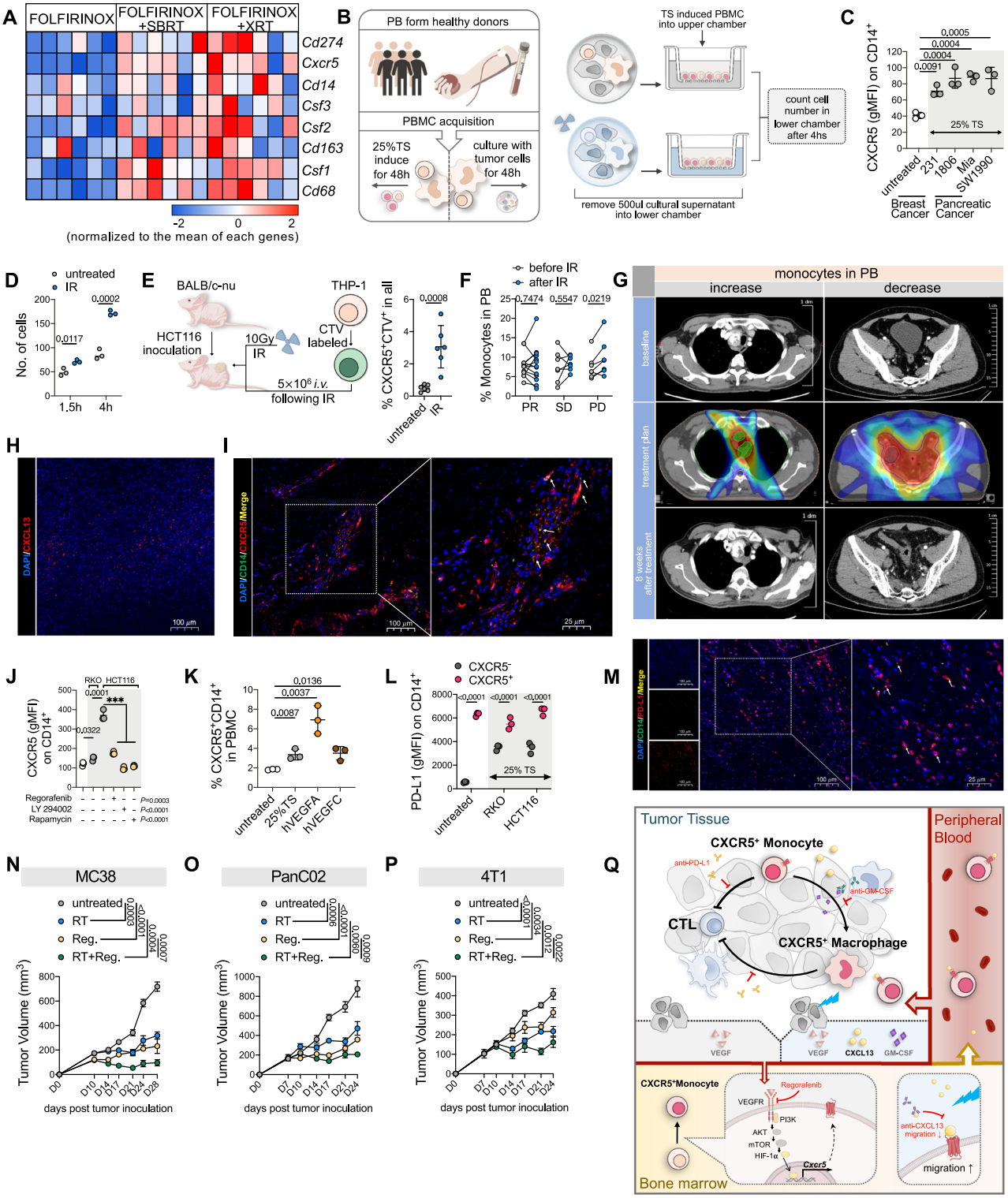

In consistent with the mouse model data, VEGFR, PI3K, or mTOR inhibitors reversed TS-induced CXCR5 expression on human monocytes (Fig. 6J). Correlation analysis of whole blood from the Genotype-Tissue Expression database revealed that CXCR5 expression was positively correlated with *Pik3r1*, *Akt1*, *Mtor*, and *Hif1a* (Supplementary Fig. 9F). PBMCs from healthy donors showed a baseline level of $CXCR5^+CD14^+$, which consistent with the findings of a previous report[44]. The proportion of $CXCR5^+CD14^+$ cells increased with human recombinant VEGF-AA treatment (Fig. 6K). In whole blood, CXCR5 expression was positively correlated with VEGFA (Supplementary Fig. 9G). PD-L1 was highly expressed on the $CXCR5^+CD14^+$ population (Fig. 6L) and was positively correlated with whole blood CXCR5 expression (Supplementary Fig. 9H). In cancer patients, PD-L1$^+$ monocytes infiltrated into tumors following radiation treatment (Fig. 6M). We next examined the quantity and immunosuppressive function of $CXCR5^+$ monocytes in tumors treated with different radiation doses and fractionation regimens at various time points following IR. Radiation-induced $CXCR5^+$ monocyte infiltration was found to be dose-dependent (Supplementary Fig. 9I); however, the radiation dose did not affect $CXCR5^+$ monocyte function

Fig. 6 | Radiation induced human CXCR5⁺ monocytes infiltration in tumor. **A** Heatmap of the mRNA expression of tumor tissue from pancreatic patients who received radiotherapy or not (GSE129492). **B** Schematic diagram of human CXCR5⁺ monocytes induction and trans-well assay. TS, tumor supernatant. PBMC, peripheral blood mononuclear cell. Created with MedPeer (medpeer.cn). **C** CXCR5 expression on monocytes cultured with 25% TS. **D** The quantity of migrated monocytes. **E** THP-1 transfer assay. CXCR5⁺CTV-labled THP-1 cells in tumor were analyzed. $n = 6$ mice/group. Created with MedPeer (medpeer.cn). **F** Monocytes in PB. PB was tested within a 7-day window before and after the radiotherapy initiation. All patients were assessed according to RECIST. $n = 13$ individuals in partial response (PR) group, $n = 14$ in stable disease (SD) group, and $n = 6$ in progressive disease (PD) group. Details are shown in Supplementary Table 4. **G** Representative CT images of patients before and after radiotherapy. (**H** and **I**) Representative immunofluorescence staining of tumor tissue from rectal cancer patients who received radiotherapy. CXCL13 (red), nuclear (blue) (**H**); CD14 (green), CXCR5 (red), nuclear (blue) (**I**). $n = 3$ individuals. **J**, **K** CXCR5 expression on monocytes. Monocytes pretreated with 1 μM regorafenib, 10 μM LY294002, and 10 μM rapamycin were cultured with TS (**J**). Monocytes were cultured with rhVEGFA and rhVEGFC (K). (L) PD-L1 expression on human CXCR5⁻ and CXCR5⁺ monocytes. **M** Representative immunofluorescence staining of tumor tissue from rectal cancer patients who received radiotherapy. CD14 (green), PD-L1 (red), nuclear (blue) (**I**). $n = 3$ individuals. **N**–**P** Tumor growth of MC38 (**N**), PanC02 (**O**), and 4T1 (**P**) tumor–bearing mice treated with IR and regorafenib. $n = 5$ mice/group. **Q** Graphical abstract of this study. Created with MedPeer (medpeer.cn). $n = 3$ cells examined over 2 independent experiments (**C**, **D**, and **J**–**L**). Statistical analysis by two-sided one-way (**C**, **J**, and **K**), or two-way (**L**–**P**) ANOVA, or unpaired (**D**, **E**) and paired (**F**) t-test. Data shown in panels (**N**–**P**) are represented as mean ± SEM, other panels are represented as mean ± SD; * $p < 0.05$; ** $p < 0.01$; *** $p < 0.001$, and NS, not significant.

(Supplementary Fig. 9J). Given that regorafenib reduced the proportion of CXCR5⁺ monocytes in a mouse model (Fig. 2Q), we investigated the therapeutic effect of combination treatment with regorafenib and RT. The results showed that regorafenib enhanced radiation-induced tumor control in the colonic, pancreatic, and breast tumor models (Fig. 6N–P). Taken together, these findings indicate that RT induces monocyte infiltration through the CXCR5–CXCL13 axis, which is correlated with a poor prognosis and is a potential candidate for enhancing the efficacy of RT.

Discussion

Tumor radioresistance is the main cause of local radiation treatment failure. The increase in immunosuppressive myeloid cells after radiation treatment is associated with weakened RT effects[12,14,45–47]. In the present study, we identified a previously unrecognized group of monocytes characterized by CXCR5 expression and elucidated the important role of CXCR5⁺ monocytes in radioresistance from the perspectives of their generation, migration, immune function, and differentiation (Fig. 6Q).

In tumor-bearing hosts, cancer mediated myelopoiesis, including Ly6C^{high} monocytes, expands and skew toward immunosuppressive properties[38]. We found that part of the expanded monocytes induced by tumors express CXCR5. We further confirmed that VEGF activated the PI3K/Akt/mTOR/HIF-1α axis in monocytes and induced CXCR5 expression. These cells highly express PD-L1 and have a strengthened immunosuppressive effect on CD8⁺ T cells. Our data showed that inhibiting VEGFR counteracted tumor-induced CXCR5⁺ monocytes and enhanced the therapeutic efficacy of radiation. These results are consistent with clinical evidence that regorafenib (a VEGFR inhibitor)[48–50] and PAM inhibition[51,52] promote CD8⁺ T-cell-induced antitumor activity.

The systemic protumor effects of radiotherapy have received growing attention in recent years. Piffko, A. et al. report that radiation induced-tumor-derived amphiregulin reprograms EGFR⁺ myeloid cells towards an immunosuppressive phenotype and promotes metastasis. The 'badscopal' proposed in this study provides an insight for re-evaluating radiotherapy's systemic impacts[53]. Our study revealed that radiation induces systemic increases in myeloid-derived suppressor cells (MDSCs), which promote distant metastasis. Studies have demonstrated that CCL2-CCR2 recruits monocytes and promotes tumor metastasis and radiation resistance[12,54]. These studies and the present investigation all focus on the radiation-induced immunosuppressive response and reveal the systemic and local protumor effects of radiation. Given that radiotherapy leads to changes in various chemokines, the role of other chemokines in radiation-induced immune responses and their underlying mechanisms requires further investigation.

A recent study demonstrated that plasma CXCL13 was higher in tumor-bearing mice than in naïve mice[55]. This finding is consistent with our results that CXCR5⁺ monocytes were increased in the PB of tumor-bearing mice compared with those in the PB of naïve mice. We found that tumor cells were the main source of radiation-induced CXCL13, and neutralizing CXCL13 inhibited CXCR5⁺ monocyte infiltration, which enhanced tumor control alone or with anti-PD-L1 during IR. These results suggest that developing a CXCL13 monoclonal antibody or exploring therapeutic targets to inhibit CXCL13 production in tumor cells is expected to improve the effect of IR. Notably, CXCL13 shows protective effects against HBV infection, and its expression is upregulated in various autoimmune diseases[56,57]. Therefore, clinical applications of anti-CXCL13 for cancer treatment should consider potential risks, including increased susceptibility to infections and interference with autoimmune disease diagnostics. Furthermore, CXCL13⁺ T cells have been reported to have antitumor effects[58,59], the impact of anti-CXCL13 on the quantity and function of CXCL13⁺ T cells necessitates further investigation. Overall, our work revealed a novel axis of monocyte migration, especially during tumor irradiation, and findings on the CXCL13–CXCR5 axis established an unrecognized mechanism of radioresistance. The recruitment of CXCR5⁺ monocytes during RT needs further verification in tumor patients.

Protumorigenic macrophages are enriched in the irradiated TME in two ways: (i) circulating tumor-associated macrophage precursors and (ii) M2 polarization in tumor tissues[60–62]. Consistent with these studies, our results partially clarified the mechanism of enhanced M2-like macrophages after irradiation from the perspective of CXCR5⁺ monocyte migration and differentiation. CXCL13 recruited CXCR5⁺ monocytes in irradiated tumors, and increased GM-CSF evoked these cells to differentiate toward CXCR5⁺ M2-like macrophages with immunosuppressive effects. CXCR5⁺ macrophages expressed more PD-L1 and strongly inhibited CD8⁺ T cells. We found that regorafenib reduced CXCR5⁺ monocyte infiltration and subsequently decreased the proportion of CXCR5⁺ macrophages and M2-like macrophages in a mouse model. This finding is consistent with that of a previous study showing that regorafenib enhances M1-directed monocyte polarization in patients with tumors[49]. Given that we demonstrated that regorafenib significantly enhances the efficacy of RT by reducing the proportion of CXCR5⁺ myeloid cells, we speculate that the inhibition of CXCR5⁺ myeloid cells may contribute to the synergistic effect of regorafenib on PD-L1 checkpoint blockade.

Mouse models and humans share broad structural similarities in structure but considerable differences in regulation, such as the proportions of leukocyte subsets, T cell co-stimulation, and antibody responses. Efficient interventions in mouse models require further validation in humanized animal models and clinical studies to confirm their efficacy in cancer patients. Encouragingly, a growing body of clinical trials evaluating the combination of regorafenib and RT is ongoing. The safety of combination strategies has been verified in tumor patients[63–65]. Their combination with nivolumab has

demonstrated early activity in patients with rectal cancer[66]. These ongoing clinical trials demonstrate the promise of combination strategies. Phase II clinical trials of PF-06835375, a CXCR5-directed antibody, are being conducted in patients with autoimmune disease[67], which has the potential to be combined with RT and to benefit tumor patients. Myelosuppression is the major complication of RT in patients with tumors[68,69]. GM-CSF treatment is widely used to rescue BM suppression in cancer patients. Our results revealed that anti-GM-CSF reduced the $CXCR5^+$M2-like macrophages and enhanced the radiation effect. These findings suggest that the potential hazard of GM-CSF treatment in the clinic should be considered.

In conclusion, we provide novel evidence that radiation induced CXCL13 production, thereby increasing the number of $CXCR5^+$ monocytes migrating from the BM and PB to the tumor. $CXCR5^+$ monocytes and macrophages impair the therapeutic efficacy of radiation by inhibiting antitumor immunity. Combining RT with regorafenib, anti-PD-L1, or anti-CXCL13 is expected to improve RT and benefit cancer patients.

Methods

Human study

All uses of human material and the clinical data of patients and PBMCs obtained from healthy donors have been approved by the Research Ethics Committee of The First Affiliated Hospital of Xi'an Jiaotong University and complied with all relevant ethical regulations. All recruited volunteers provided written informed consent.

Mice

All animal experiments were performed in accordance with protocols approved by the Xi'an Jiantong University Institutional Animal Care and Use Committee (IACUC). All animals were maintained in pathogen-free conditions and cared for in accordance with the International Association for Assessment and Accreditation of Laboratory Animal Care policies and certification. Mice were euthanized by carbon dioxide (CO_2) asphyxiation at the end point. Wild-type C57BL/6 (N000013), BALB/c (N000020), and BALB/c-nu (D000521) were purchased from GemPharmatech and Laboratory Animal Center of Xi'an Jiaotong University Health Science Center. CD45.1.2 strain was kindly provided by Zhang's lab[70]. C57BL/6 $CXCR5^{-/-}$ strain (S-KO-01232) was purchased from Cyagen. The mice aged six to eight weeks were used in the experiments. Experimental and control animals were bred separately. All WT mice were randomly grouped. Given the nature of the transgenic mice, grouping was not random but rather based on their genotypes. However, the age and the weight of the mice was equally distributed.

Tumor growth and treatment

To establish subcutaneous tumor model, 1.5×10^6 tumor cells were subcutaneously (*s.c.*) injected in the right flank of mice. Tumors were measured twice weekly for 3–4 weeks (length × width × depth/2). Mice were pooled and randomly divided into different groups at 10 days after tumor inoculation (tumor volume reached ~100 mm^3). In accordance with the approved protocol of IACUC, the maximum tumor volume was set at 1500 mm^3. No tumors in this study exceeded this limit, and animals were euthanized upon reaching this endpoint or if any signs of distress were observed. For IR treatment, X-ray radiation (225 keV, dose rate 3.072 Gy/min) was delivered to the tumors using a RS2000pro irradiation system (American). Tumors were irradiated at 10 days post tumor inoculation with one dose of 12 Gy. All irradiated mice were shielded under anesthesia.

For rmVEGF treatment, 175 μg/kg of rmVEGF (450-32, PeproTech) was injected intraperitoneally to naïve mice every other day for 4 times in total. For anti-VEGF-A treatment, 5 mg/kg InVivoMAb anti-mouse VEGF-A (BE0399, BioXcell) was injected intraperitoneally on the 7 days after tumor inoculation every other day for 4 times in total. For regorafenib treatment experiment, 10 mg/kg regorafenib (HY-10331, MCE) was given by gavage daily starting 3 days before IR for a total of 14 times. For CCR5 and CXCR3 antagonist, 5 mg/kg TAK-220 (HY-19974, MCE) or 15 mg/kg AMG 487 (HY-15319, MCE) was given by gavage on the day of IR and every other day thereafter till endpoint. For CXCL13 neutralization experiment, 2 μg antibody (MAB470-100, R&D) was injected intratumorally every other day starting on the day of IR for a total of 5 times. For mono-mac depletion, 25 mg/kg Invivo anti-mouse CSF1R Recombinant mAb (S0B1139, STARTER) was injected intratumorally on the day of IR and every other day thereafter till endpoint. For $CD8^+$ T cell depletion experiment, 7.5 mg/kg of antibody (BE0004-1, BioXcell) was injected intraperitoneally every three days starting 1 day before IR for a total of 4 times. For anti-PD-L1 treatment experiment, 7.5 mg/kg antibody (BE0101, BioXcell) was injected intraperitoneally every three days starting on the day of IR for a total of three times. For GM-CSF neutralization experiment, 2 μg/tumor antibody (A2148, Selleck) was injected intratumorally every other day starting on the day of IR for a total of 6 times.

For rechallenge model, more than 4 weeks after tumor regression, 5×10^5 cancer cells were injected into the left flank. For monocytes transfer experiment, 5×10^6 $CXCR5^+$ or $CXCR5^-$ monocytes were injected intravenously every three days starting on the day of IR treatment for a total of 4 times. For THP-1 transfer assay, BALB/c-nu mice were inoculated with HCT116. Ten days after tumor inoculation, tumor received 10 Gy radiation and 5×10^6 CTV-labeled THP-1 intravenous injection. Tumor were separated 3 days after radiation and analyzed by flow cytometry.

Cell lines

Murine tumor cell lines, HCT116 (SCSP-5076), RKO (SCSP-5236), Mia (SCSP-568), 1806 (SCSP-5019), and SW1990 (SCSP-5302) were purchased from Cell Resource Center, Institute of Basic Medical Sciences, Chinese Academy of Medical Sciences, Peking Union Medical College. 231 was gift of Jiao's lab[71]. All cell lines were grown in Dulbecco's modified Eagle's high glucose medium (C11995500BT, Gibco) containing 10% heat-inactivated fetal bovine serum (FBS, 12B108, EXcell), 1% Penicillin/Streptomycin (P/S, G4003, Servicebio), and were maintained in a humidified incubator with 5% CO_2 at 37 °C. Tumor supernatant was collected after 24 h culture.

Flow cytometry analysis of cell surface and intracellular protein expression

For flow cytometry analysis, tumors, blood, or bone marrow were collected from mice. Tumor tissues were cut into small pieces and incubated with 1 mg/ml collagenase IV (11088866001, Sigma) and 0.2 mg/ml deoxyribonuclease I (D8070, Sigma) for 1 h at 37 °C. Samples were then filtered through a 50 μm nylon strainer and washed twice with staining buffer (phosphate-buffered saline supplemented with 2% FBS). Peripheral blood was collected using heparin as the anticoagulant and lysed by double distilled H_2O. Bone marrow from femur was flushed with 6 ml of phosphate-buffered saline (PBS). After centrifugation, the cell pellet was incubated in Red Blood Cell Lysis buffer (r90003, Biosharp) and neutralized by staining buffer. The cells were re-suspended in staining buffer and blocked with anti-FcR (2.4G2, BioXcell). For cell surface staining, the cells were incubated with 200-fold diluted fluorescence-labeled antibodies for 45 min at 4 °C in the dark and then detected by flow cytometry with a BD Celesta. For intracellular staining, 3×10^5 cells were cultured in complete Roswell Park Memorial Institute (RPMI) 1640 medium (C11875500BT, Gibco) with Cell Stimulation Cocktail (00-4970-93, eBioscience) and Protein Transport Inhibitor Cocktail (00-4980-93, eBioscience) in 96-well plates. Five hours later, cells were harvested and fixed with Fixation Buffer (554722, BD) for 60 min on ice, and then washed twice with diluted Permeabilization Buffer (554723, BD). The appropriate antibodies were added to cells and incubated at 4 °C. The antibodies

involved in this study are summarized in Supplementary Table 1. Data were analyzed by FlowJo software.

Bone marrow derived monocytes/macrophages culture and treatment

Single-cell suspensions of bone marrow cells were obtained from wild-type or *Cxcr5*-KO C57BL/6 mice. The cells were cultured in induce medium, RPMI 1640 medium containing 10% FBS (C04002-500, VivaCell) and 20 ng/ml murine recombinant GM-CSF (96-315-03, PeproTech), at day 0. Fresh induce medium was added at day 3 and day 5. The bone marrow (BM)-derived monocytes and macrophages were obtained at day 4 and day 7.

To detect CXCR5 expression on monocytes and macrophages, cells were cultured with 25% tumor supernatant (TS) or treated with murine recombinant protein for 24 h. Monocytes pretreated with inhibitors for 30 min, and then cultured with 25% TS and the inhibitors.

To obtain $CXCR5^-$ and $CXCR5^+$ monocytes, BM-derived monocytes were cultured with 50% TS for 48 h. To obtain $CXCR5^+$ macrophages, $CXCR5^+$ monocytes were cultured in induce medium for 3 days. These two subpopulations were separated by fluorescence-activated cell sorting. To track the differentiation of $CXCR5^+$ monocytes, TS-induced monocytes were stained with APC-Cy7 labeled CXCR5. After that, all of monocytes kept cultured in induce media for 72 h. Finally, all cells were collected, stained, and then analyzed by flow cytometry.

Human PBMCs separation and treatment

Peripheral blood was freshly collected in heparin coated tube and then separated by Human Lymphocyte Separation Medium (7111011, Dakewe) in accordance with the manufacturer's instructions. To detect CXCR5 expression on monocytes, PBMCs were cultured with 25% TS or treated with human recombinant protein for 24 h. In transwell migration assay, PBMC and tumor cells were co-cultured for 2 h, and then received 10 Gy radiation or not. 48 h later, supernatant was collected. After filtering with 0.22 μM filter, 500 μl supernatant was added into lower chamber. 3×10^5 TS-treated PBMC in complete RPMI medium were added to the upper chamber. After 1.5 h and 4 h incubating, migrated cells in bottom chamber were collected and counted.

RNA interference and sgRNA-mediated gene deletion

Nonspecific control siRNA and siRNAs for HIF1α, Maf, and eIF4G2 were purchased from Sangon Biotech (China). siRNA transfection of cells was performed with Lipofectamine RNAiMAX Transfection Reagent following the manufacturer's instructions. Single-guide RNAs (sgRNAs) were designed using the Benchling online tool (https://benchling.com/) and cloned into the lentiCRISPRv2 (52961). Lentivirus production involved the co-transfection of 293 T cells using the lentiCRISPRv2 alongside psPAX2 and pMD2.G packaging plasmids. For effective viral infection, MC38 cell line was treated with the lentivirus amid the presence of 8 μg/mL polybrene, followed by a stringent selection process using 1 μg/ml puromycin for a duration of 4–6 days. Sequences of siRNA and sgRNA oligonucleotides used in this study are summarized in Supplementary Table 2.

T-cell activation assay

Bone marrow derived monocytes and macrophages were performed for the suppression assay. T cells were harvested from the lymph nodes of naïve mice and then stained with CellTrace Violet (C34557, Invitrogen). The CTV-labeled T cells (2×10^5 per well) were cultured in plate-bound 5 μg/ml of anti-CD3 (clone 145-2C11; Thermo Fisher Scientific) and 2 μg/ml of anti-CD28 (Clone 37.51; Thermo Fisher Scientific) with complete RPMI medium containing 5 μM β-mercaptoethano. $CXCR5^-$ and $CXCR5^+$ monocytes or macrophages were then added into T cell cultures at a ratio of 1:8 (myeloid cells:T cells) for 72 h. Anti-PD-L1 was added into $CXCR5^+$ monocytes for the concentration of 1 μg/ml and incubated for 30 min. Incubated $CXCR5^+$ monocytes were then cultured with T cells at a ratio of 1:8 (monocytes:T cells) with 1 μg/ml of anti-PD-L1, 5 μg/ml of anti-CD3, and 2 μg/ml of anti-CD28 as previously mentioned for 72 h. Cells were then harvested, and CTV-negative signal in the $CD8^+$ and $CD4^+$ gate was measured by flow cytometry.

Transwell migration assay

We used 24-well transwell plates with 6 mm inserts in polyethylene terephthalate track-etched membranes (Corning). Tumor was precisely weighed (100 ± 0.5 mg), then grinded and centrifuged at $13000 \times g$ for 15 min. The supernatant was collected and added to bottom chamber. The tumor homogenate culture medium was comprised by 40% supernatant and 60% complete medium of RPMI for 500 μl in total. In ex vivo CXCL13 neutralization assay, the supernatant of homogenate from the same irradiated tumor was divided into two parts, one of which was pretreated with 150 ng/ml anti-CXCL13 for 30 min. After that, the supernatant was added to bottom chamber. The tumor homogenate culture medium was comprised as previously mentioned and 150 ng/ml anti-CXCL13. 3×10^5 TS-treated monocytes in complete RPMI medium were added to the upper chamber. After 4 h incubating, migrated cells in bottom chamber were collected, counted, and then analyzed by flow cytometry.

Cytometric bead array

For tumor chemokines and cytokines quantifications, tumor tissues were homogenized in PBS with protease inhibitor followed by addition of Triton X-100. The LEGENDplex MU Proinflam Chemokine Panel (Biolegend) and the LEGENDplex Mouse Inflammation Panel (Biolegend) were used for quantitative analysis of CXCL1, CCL5, CCL20, CCL11, CCL17, CCL2, CXCL9, CXCL10, CCL3, CCL4, CXCL13, CXCL5, CCL22, IL-23, IL-1α, IFN-γ, TNF, MCP-1, IL-12p70, IL-1β, IL-10, IL-6, IL-27, IL-17A, IFN-β, and GM-CSF in accordance with the manufacturer's instructions.

Western blot analysis

Whole-cell protein was extracted with Triton X-100 buffer (150 mM sodium chloride, 50 mM Tris, 1% Triton X-100; pH 8.0) with proteinase inhibitors and phosphatase inhibitors (HY-K0010, HY-K0021, MCE). Immuno-blotting analyses were performed as previously described[9]. Primary antibodies against the following proteins were utilized in this study: PI3K (A4992, ABclonal), p-PI3K (AP0854, ABclonal), AKT (A18675, ABclonal), p-AKT (AP0637, ABclonal), mTOR (2983 T, CST), p-mTOR (5536 T, CST), HIF1α (36169 T, CST), Maf (A3361, ABclonal), and eIF4G (A2897, ABclonal). Horseradish peroxidase-linked anti-rabbit (78430, Thermofisher) secondary antibody was used. GAPDH mAb (A19056, ABclonal) was used to normalize for the amount of loaded protein.

Immunofluorescence and confocal imaging

Tumor tissues were separated and embedded in Optimal Cutting Temperature Compound. The cyoblock was cut at a thickness of 5 μm and washed with PBS for 10 min. The cryosection was permeabilized with 0.5% Triton X-100 for 20 min and blocked with 10% normal goat serum for 1 h at room temperature. The samples were incubated with PE anti-mouse CD45 (Clone 30-F11; Biolegend), FITC anti-mouse Ly6C (Clone HK1.4; BioLegend), APC/Fire 750 anti-mouse CD185 (Clone L138D7; BioLegend), APC anti-mouse CXCL13 (Clone DS8CX1; Ebioscience). The cryosections were then thoroughly washed with PBS and counterstained with DAPI (D8417, Sigma). Regarding formalin-fixed paraffin-embedded tissue section, the section was deparaffinized and rehydrated before antigen retrieval. After serum blocking (as previously mentioned), the samples were incubated with anti-human CD14 (Clone HCD14; BioLegend), CXCR5 (Clone J252D4; BioLegend), CXCL13 (orb13426, biorbyt), and PD-L1 (66248, proteintech) overnight at 4 °C. The slides were then thoroughly washed with PBS and

incubated with secondary antibody at room temperature for 50 min in the dark. DAPI counterstain is same as previously mentioned. Images were acquired on an Olympus FV3000 confocal microscope. Image analysis was performed using Image J.

Hematoxylin-eosin (HE) staining

Tumor tissue sections embedded in paraffin were stained with haematoxylin and eosin (HE) in accordance with the manufacturer's protocol. Following deparaffinisation, the sections were stained with Mayer's haematoxylin. After differentiation using a hydrochloric acid and alcohol solution, followed by ammonia treatment, the sections were stained with eosin.

RT–qPCR analysis

RNA was extracted from the cells using TRIzol (P118-05, GenStar) or RNeasy Mini Kit (74804, QIAGEN), treated with DNase using a TURBO DNA-free Kit (AM1907, Thermofisher) or an RNase-Free DNase Set (11119915001, Sigma), and transcribed into cDNA using the High-Capacity cDNA Reverse Transcription Kit (205311, Qiagen). PCR was performed using SYBR green (RK21203, Yeasen) with specific primers (Supplementary Table 3). Reactions were run on an ABI QuantStudio 5 Real-time PCR System (Thermo Fisher Scientific). The cycling conditions were as follows: (a) 95 °C 3 min, 1 cycle; (b) 95 °C 5 secs, followed by 60 °C 30 secs, 40 cycles. Following the amplification, the Ct values for target genes and the reference gene, GAPDH, were recorded. Fold induction was calculated using the ΔΔCt method.

Bulk RNA-seq analysis

The total RNA was extracted according to the instructions manual of the TRIzol Reagent (Life Technologies). RNA concentration and purity were measured using NanoDrop 2000 (Thermo Fisher Scientific). RNA integrity was assessed using the RNA Nano 6000 Assay Kit of the Agilent Bioanalyzer 2100 system (Agilent Technologies). A total amount of 1 μg RNA per sample was used as input material for the RNA sample preparations. Sequencing libraries were generated using Hieff NGS Ultima Dual-mode mRNA Library Prep Kit for Illumina (Yeasen Biotechnology (Shanghai) Co., Ltd.) following manufacturer's recommendations, and index codes were added to attribute sequences to each sample. Raw data (raw reads) of fastq format were firstly processed through in-house perl scripts. In this step, clean data (clean reads) were obtained by removing reads containing adapter, reads containing ploy-N and low-quality reads from raw data. At the same time, Q20, Q30, GC-content, and sequence duplication level of the clean data were calculated. All the downstream analyses were based on clean data with high quality. The StringTie Reference Annotation Based Transcript assembly method was used to construct and identify both known and novel transcripts from Hisat2 alignment results. Gene function was annotated based on the KEGG Ortholog database and Gene Ontology. Gene expression levels were estimated by fragments per kilobase of transcript per million fragments mapped. Differential expression analysis of two conditions/groups was performed using the DESeq2. The resulting *P* values were adjusted using the Benjamini and Hochberg's approach for controlling the false discovery rate. Genes with an adjusted *P*-value < 0.01 & Fold Change≥2 found by DESeq2 were assigned as differentially expressed. Differential expression analysis of two samples was performed using the edgeR. The FDR < 0.01 & Fold Change ≥2 was set as the threshold for significantly differential expression.

TCGA data analysis

TCGA data were acquired and analyzed by the Gene Expression Profiling Interactive Analysis Platform. The mRNA expression of tumors was analyzed by the Multiple Gene Comparison module. The overall survival of rectum adenocarcinoma, colon adenocarcinoma, pancreatic adenocarcinoma, and breast invasive carcinoma was analyzed by the Kaplan-Meier estimator and tested by the log rank using the survival module.

Statistics and reproducibility

Analyses were performed using GraphPad Prism Version 9.0.0. Data were analyzed by one-way ANOVA with Tukey's Multiple Comparison Test or Student's t test. All statistical tests were two-sided. *P* values < 0.05 were considered statistically significant (ns > 0.05, $^{*}p < 0.05$, $^{**}p < 0.01$, $^{***}p < 0.001$). The in vitro experiments have been repeated at least twice. The in vivo experiments have been performed in at least two to three independent batches or have at a minimum 5–10 independent biological replicates for reproducibility. For Fig. 6H, I, and M, the experiments have been performed in 3 individuals and repeated twice.

Reporting summary

Further information on research design is available in the Nature Portfolio Reporting Summary linked to this article.

Data availability

The mRNA-seq data generated in this study have been deposited in the SRA database under the [PRJNA1420777] [https://www.ncbi.nlm.nih.gov/sra/PRJNA1420777]. All data are included in the Supplementary Information or available from the authors, as are unique reagents used in this Article. The raw numbers for charts and graphs are available in the Source Data file whenever possible. Source data are provided with this paper.

References

1. Weichselbaum, R. R., Liang, H., Deng, L. & Fu, Y. X. Radiotherapy and immunotherapy: a beneficial liaison? *Nat. Rev. Clin. Oncol.* **14**, 365–379 (2017).
2. Zhang, Z., Liu, X., Chen, D. & Yu, J. Radiotherapy combined with immunotherapy: the dawn of cancer treatment. *Signal Transduct. Target Ther.* **7**, 258 (2022).
3. Schaue, D. & McBride, W. H. Opportunities and challenges of radiotherapy for treating cancer. *Nat. Rev. Clin. Oncol.* **12**, 527–540 (2015).
4. Barnett, G. C. et al. Normal tissue reactions to radiotherapy: towards tailoring treatment dose by genotype. *Nat. Rev. Cancer* **9**, 134–142 (2009).
5. Huang, R. X. & Zhou, P. K. DNA damage response signaling pathways and targets for radiotherapy sensitization in cancer. *Signal Transduct. Target Ther.* **5**, 60 (2020).
6. Steinbichler, T. B. et al. Therapy resistance mediated by exosomes. *Mol. Cancer* **18**, 58 (2019).
7. Formenti, S. C. & Demaria, S. Radiation therapy to convert the tumor into an in situ vaccine. *Int J. Radiat. Oncol. Biol. Phys.* **84**, 879–880 (2012).
8. Raskov, H., Orhan, A., Christensen, J. P. & Gogenur, I. Cytotoxic CD8(+) T cells in cancer and cancer immunotherapy. *Br. J. Cancer* **124**, 359–367 (2021).
9. Hou, Y. et al. Non-canonical NF-kappaB antagonizes STING sensor-mediated DNA sensing in radiotherapy. *Immunity* **49**, 490–503 e494 (2018).
10. Hou, Y. et al. Radiotherapy enhances metastasis through immune suppression by inducing PD-L1 and MDSC in distal sites. *Clin. Cancer Res* **30**, 1945–1958 (2024).
11. Deng, L. et al. Irradiation and anti-PD-L1 treatment synergistically promote antitumor immunity in mice. *J. Clin. Investig.* **124**, 687–695 (2014).
12. Liang, H. et al. Host STING-dependent MDSC mobilization drives extrinsic radiation resistance. *Nat. Commun.* **8**, 1736 (2017).
13. Demaria, S., Golden, E. B. & Formenti, S. C. Role of local radiation therapy in cancer immunotherapy. *JAMA Oncol.* **1**, 1325–1332 (2015).

14. Wang, L. et al. YTHDF2 inhibition potentiates radiotherapy antitumor efficacy. *Cancer Cell* **41**, 1294–1308 e1298 (2023).
15. Cassetta, L. et al. Human tumor-associated macrophage and monocyte transcriptional landscapes reveal cancer-specific reprogramming, biomarkers, and therapeutic targets. *Cancer Cell* **35**, 588–602 e510 (2019).
16. Guo, S., Chen, X., Guo, C. & Wang, W. Tumour-associated macrophages heterogeneity drives resistance to clinical therapy. *Expert Rev. Mol. Med.* **24**, e17 (2022).
17. Gabrilovich, D. I. & Nagaraj, S. Myeloid-derived suppressor cells as regulators of the immune system. *Nat. Rev. Immunol.* **9**, 162–174 (2009).
18. Yi, M. et al. Combination strategies with PD-1/PD-L1 blockade: current advances and future directions. *Mol. Cancer* **21**, 28 (2022).
19. Gong, J., Le, T. Q., Massarelli, E., Hendifar, A. E. & Tuli, R. Radiation therapy and PD-1/PD-L1 blockade: the clinical development of an evolving anticancer combination. *J. Immunother. Cancer* **6**, 46 (2018).
20. Nagarsheth, N., Wicha, M. S. & Zou, W. Chemokines in the cancer microenvironment and their relevance in cancer immunotherapy. *Nat. Rev. Immunol.* **17**, 559–572 (2017).
21. Ren, J. et al. CXCL13 as a Novel Immune Checkpoint for Regulatory B Cells and Its Role in Tumor Metastasis. *J. Immunol.* **208**, 2425–2435 (2022).
22. Qi, X. W. et al. Expression features of CXCR5 and its ligand, CXCL13 associated with poor prognosis of advanced colorectal cancer. *Eur. Rev. Med. Pharm. Sci.* **18**, 1916–1924 (2014).
23. Biswas, S. et al. CXCL13-CXCR5 co-expression regulates epithelial to mesenchymal transition of breast cancer cells during lymph node metastasis. *Breast Cancer Res. Treat.* **143**, 265–276 (2014).
24. Liu, X. et al. Transcription factor achaete-scute homologue 2 initiates follicular T-helper-cell development. *Nature* **507**, 513–518 (2014).
25. Gu, X. et al. Revisiting the CXCL13/CXCR5 axis in the tumor microenvironment in the era of single-cell omics: Implications for immunotherapy. *Cancer Lett.* **605**, 217278 (2024).
26. Halvorsen, B. et al. Activated platelets promote increased monocyte expression of CXCR5 through prostaglandin E2-related mechanisms and enhance the anti-inflammatory effects of CXCL13. *Atherosclerosis* **234**, 352–359 (2014).
27. Biswas, S. et al. RelA driven co-expression of CXCL13 and CXCR5 is governed by a multifaceted transcriptional program regulating breast cancer progression. *Biochim. Biophys. Acta Mol. Basis Dis.* **1865**, 502–511 (2019).
28. Wan, S. et al. Costimulation molecules differentially regulate the ERK-Zfp831 axis to shape T follicular helper cell differentiation. *Immunity* **54**, 2740–2755 e2746 (2021).
29. Pan, T. et al. Immune effects of PI3K/Akt/HIF-1alpha-regulated glycolysis in polymorphonuclear neutrophils during sepsis. *Crit. Care* **26**, 29 (2022).
30. Li, D. et al. beta2-microglobulin maintains glioblastoma stem cells and induces M2-like polarization of tumor-associated macrophages. *Cancer Res.* **82**, 3321–3334 (2022).
31. Palombo, R. et al. Inhibition of the PI3K/AKT/mTOR signaling promotes an M1 macrophage switch by repressing the ATF3-CXCL8 axis in Ewing sarcoma. *Cancer Lett.* **555**, 216042 (2023).
32. Weichhart, T. & Saemann, M. D. The PI3K/Akt/mTOR pathway in innate immune cells: emerging therapeutic applications. *Ann. Rheum. Dis.* **67**, iii70–iii74 (2008).
33. Chi, H. Regulation and function of mTOR signalling in T cell fate decisions. *Nat. Rev. Immunol.* **12**, 325–338 (2012).
34. Saxton, R. A. & Sabatini, D. M. mTOR signaling in growth, metabolism, and disease. *Cell* **168**, 960–976 (2017).
35. Panwar, V. et al. Multifaceted role of mTOR (mammalian target of rapamycin) signaling pathway in human health and disease. *Signal Transduct. Target Ther.* **8**, 375 (2023).
36. Chen, K., Zhu, L., Guo, L., Pan, Y. B. & Feng, D. F. Maf1 regulates dendritic morphogenesis and influences learning and memory. *Cell Death Dis.* **11**, 606 (2020).
37. Porta, C. et al. Tumor-derived prostaglandin E2 promotes p50 NF-kappaB-dependent differentiation of monocytic MDSCs. *Cancer Res.* **80**, 2874–2888 (2020).
38. Christofides, A. et al. The complex role of tumor-infiltrating macrophages. *Nat. Immunol.* **23**, 1148–1156 (2022).
39. Cervantes-Villagrana, R. D., Albores-Garcia, D., Cervantes-Villagrana, A. R. & Garcia-Acevez, S. J. Tumor-induced neurogenesis and immune evasion as targets of innovative anti-cancer therapies. *Signal Transduct. Target Ther.* **5**, 99 (2020).
40. Whiteside, T. L. Inhibiting the inhibitors: evaluating agents targeting cancer immunosuppression. *Expert Opin. Biol. Ther.* **10**, 1019–1035 (2010).
41. Kabashima, K. et al. Thromboxane A2 modulates interaction of dendritic cells and T cells and regulates acquired immunity. *Nat. Immunol.* **4**, 694–701 (2003).
42. Parker, K. H., Beury, D. W. & Ostrand-Rosenberg, S. Myeloid-derived suppressor cells: critical cells driving immune suppression in the tumor microenvironment. *Adv. Cancer Res* **128**, 95–139 (2015).
43. Raines, L. N. et al. PERK is a critical metabolic hub for immunosuppressive function in macrophages. *Nat. Immunol.* **23**, 431–445 (2022).
44. Li, C. et al. Comprehensive analysis of human monocyte subsets using full-spectrum flow cytometry and hierarchical marker clustering. *Front. Immunol.* **15**, 1405249 (2024).
45. Oweida, A. J. et al. Response to radiotherapy in pancreatic ductal adenocarcinoma is enhanced by inhibition of myeloid-derived suppressor cells using STAT3 anti-sense oligonucleotide. *Cancer Immunol. Immunother.* **70**, 989–1000 (2021).
46. Sridharan, V. et al. Definitive chemoradiation alters the immunologic landscape and immune checkpoints in head and neck cancer. *Br. J. Cancer* **115**, 252–260 (2016).
47. Tsai, M. S., Chen, W. C., Lai, C. H., Chen, Y. Y. & Chen, M. F. Epigenetic therapy regulates the expression of ALDH1 and immunologic response: Relevance to the prognosis of oral cancer. *Oral. Oncol.* **73**, 88–96 (2017).
48. Fukuoka, S. et al. Regorafenib plus nivolumab in patients with advanced gastric or colorectal cancer: an open-label, dose-escalation, and dose-expansion phase Ib trial (REGONIVO, EPOC1603). *J. Clin. Oncol.* **38**, 2053–2061 (2020).
49. Kim, H. D. et al. Regorafenib plus nivolumab in unresectable hepatocellular carcinoma: the phase 2 RENOBATE trial. *Nat. Med.* **30**, 699–707 (2024).
50. Fakih, M. et al. Regorafenib plus nivolumab in patients with mismatch repair-proficient/microsatellite stable metastatic colorectal cancer: a single-arm, open-label, multicentre phase 2 study. *EClinicalMedicine* **58**, 101917 (2023).
51. Lanahan, S. M., Wymann, M. P. & Lucas, C. L. The role of PI3Kgamma in the immune system: new insights and translational implications. *Nat. Rev. Immunol.* **22**, 687–700 (2022).
52. Glaviano, A. et al. PI3K/AKT/mTOR signaling transduction pathway and targeted therapies in cancer. *Mol. Cancer* **22**, 138 (2023).
53. Piffko, A. et al. Radiation-induced amphiregulin drives tumour metastasis. *Nature* **643**, 810–819 (2025).
54. Qian, B. Z. et al. CCL2 recruits inflammatory monocytes to facilitate breast-tumour metastasis. *Nature* **475**, 222–225 (2011).
55. Lucotti, S. et al. Extracellular vesicles from the lung pro-thrombotic niche drive cancer-associated thrombosis and metastasis via integrin beta 2. *Cell*, https://doi.org/10.1016/j.cell.2025.01.025 (2025).

56. Hui, L., Li, Y., Huang, M. K., Jiang, Y. M. & Liu, T. CXCL13: a common target for immune-mediated inflammatory diseases. *Clin. Exp. Med.* **24**, 244 (2024).
57. Li, Y. et al. CXCL13-mediated recruitment of intrahepatic CXCR5(+) CD8(+) T cells favors viral control in chronic HBV infection. *J. Hepatol.* **72**, 420–430 (2020).
58. Wang, F. et al. Single-cell and spatial transcriptome analysis reveals the cellular heterogeneity of liver metastatic colorectal cancer. *Sci. Adv.* **9**, eadf5464 (2023).
59. Wu, Z. X. et al. CD69(+)CD103(+)CD8(+) tissue-resident memory T cells possess stronger anti-tumor activity and predict better prognosis in colorectal cancer. *Cell Commun. Signal* **22**, 608 (2024).
60. Ni, H. et al. FLASH radiation reprograms lipid metabolism and macrophage immunity and sensitizes medulloblastoma to CAR-T cell therapy. *Nat. Cancer*, https://doi.org/10.1038/s43018-025-00905-6 (2025).
61. Guo, S. et al. Radiation-induced tumor immune microenvironments and potential targets for combination therapy. *Signal Transduct. Target Ther.* **8**, 205 (2023).
62. Rodriguez-Ruiz, M. E., Vitale, I., Harrington, K. J., Melero, I. & Galluzzi, L. Immunological impact of cell death signaling driven by radiation on the tumor microenvironment. *Nat. Immunol.* **21**, 120–134 (2020).
63. Gregucci, F. et al. Reirradiation with radiosurgery or stereotactic fractionated radiotherapy in association with regorafenib in recurrent glioblastoma. *Strahlenther. Onkol.* **200**, 751–759 (2024).
64. Kennedy, A. et al. Regorafenib prior to selective internal radiation therapy using (90)Y-resin microspheres for refractory metastatic colorectal cancer liver metastases: analysis of safety, dosimetry, and molecular markers. *Front. Oncol.* **9**, 624 (2019).
65. Zhou, S. et al. Regorafenib alone or in combination with high/low-dose radiotherapy plus toripalimab as third-line treatment in patients with metastatic colorectal cancer: protocol for a prospective, randomized, controlled phase II clinical trial (SLOT). *Front. Oncol.* **13**, 1274487 (2023).
66. Bregni, G. et al. Rationale and design of REGINA, a phase II trial of neoadjuvant regorafenib, nivolumab, and short-course radiotherapy in stage II and III rectal cancer. *Acta Oncol.* **60**, 549–553 (2021).
67. Cohen, S. et al. A Phase 1, randomized, double-blind, placebo-controlled, single- and multiple-dose escalation study to evaluate the safety and pharmacokinetics/pharmacodynamics of PF-06835375, a C-X-C chemokine receptor type 5 directed antibody, in patients with systemic lupus erythematosus or rheumatoid arthritis. *Arthritis Res. Ther.* **26**, 117 (2024).
68. Le Rhun, E. et al. Prognostic significance of therapy-induced myelosuppression in newly diagnosed glioblastoma. *Neuro Oncol.* **24**, 1533–1545 (2022).
69. Mauch, P. et al. Hematopoietic stem cell compartment: acute and late effects of radiation therapy and chemotherapy. *Int. J. Radiat. Oncol. Biol. Phys.* **31**, 1319–1339 (1995).
70. Zhang, Z. et al. Trappc1 intrinsically prevents ferroptosis of naive T cells to avoid spontaneous autoinflammatory disease in mice. *Eur. J. Immunol.* **54**, e2350836 (2024).
71. Gong, L. et al. CK2-mediated phosphorylation of SUZ12 promotes PRC2 function by stabilizing enzyme active site. *Nat. Commun.* **13**, 6781 (2022).

Acknowledgements

This study was supported by the National Natural Science Foundation of China (82273194, 82472812 and 82073176 to Y Hou, 82203120 to S Huang) and Natural Science Foundation of Shaanxi Province (2025JC-JCQN-100 to Y Hou). We thank Yi Li, Jing Wang, Luping Zhou, and Jue Lu of Department of Radiation Oncology, The First Affiliated Hospital of Xi'an Jiaotong University for helpful discussions and their professional support. We thank Qi Wang and Xuehui Luo for their help for the peripheral blood processing. We thank teachers Xiaofei Wang and Wen Li of Biomedical Experimental Center of Xi'an Jiaotong University and senior engineer Lai Baochang of Xi'an Jiaotong University for their professional technical support. We thank Laboratory Animal Center of Xi'an Jiaotong University for their assistance with experimental mice and mice breeding. We thank LetPub (www.letpub.com.cn) for its linguistic assistance during the preparation of this manuscript.

Author contributions

Y.L. and R.J. performed most of the experiments. Y.L. and C.C. analyzed the data. Y.L., R.J., and C.C. wrote the manuscript. P.C., Y.W., and J Sun performed western blot and partial cell experiments. P.C. performed the mice genotyping. J. Shi, M.H., Q.M., M.S., D.J., T.L., and R.W. helped to perform animal experiments. M.H. helped to perform partial cell experiments. D.H. and M.S. helped to perform RT-qRNA. M.H., R.D., and W.L. helped to perform Fluorescence Activated Cell Sorting. F.W. and D.Y. helped to analyze the RNA sequencing data. H.L., A.J., H.T., S.H., J.L., and M.C. helped to conduct experiments. R.G., J.Z., Y.W., and Y.S. helped to collect clinical data. L.Y., L.H., C.H., and C.L. provided clinical guidance for the research. Y.H., S.H., and J.M. designed and supervised the study.

Competing interests

The authors declare no competing interests.

Additional information

Supplementary information The online version contains supplementary material available at https://doi.org/10.1038/s41467-026-70858-6.

Correspondence and requests for materials should be addressed to Jinlu Ma, Suxia Han or Yuzhu Hou.

Peer review information *Nature Communications* thanks the anonymous reviewer(s) for their contribution to the peer review of this work. A peer review file is available.

[1]Department of Radiation Oncology, First Affiliated Hospital of Xi'an Jiaotong University, Xi'an, Shaanxi, China. [2]Department of Pathogenic Microbiology and Immunology, School of Basic Medical Sciences, Xi'an Jiaotong University, Xi'an, Shaanxi, China. [3]Department of Pathology, School of Basic Medical Sciences, Xi'an Jiaotong University, Xi'an, Shaanxi, China. [4]Daily-surgery center, First Affiliated Hospital of Xi'an Jiaotong University, Xi'an, Shaanxi, China. [5]Institute of Infection and Immunity, Translational Medicine Institute, Xi'an Jiaotong University Health Science Center, Xi'an, Shaanxi, China. [6]Department of Laboratory Medicine, First Affiliated Hospital of Xi'an Jiaotong University, Xi'an, Shaanxi, China. [7]Department of pathology, First Affiliated Hospital of Xi'an Jiaotong University, Xi'an, Shaanxi, China. [8]Department of Radiation Oncology, The Second Affiliated Hospital of Xi'an Jiaotong University, Xi'An, China. [9]Department of General Surgery, Peking Union Medical College Hospital, Chinese Academy of Medical Sciences, Beijing, China. [10]Genome Insitute, the First Affiliated Hospital of Xi'an Jiaotong University, Xi'an, Shaanxi, China. [11]Shaanxi Key Laboratory of Medical Superconducting Heavy Ion Accelerator and Radiomedicine, Xi'an, Shaanxi, China. [12]MOE Key Laboratory of Environment and Genes Related to Diseases, School of Medicine, Xi'an Jiaotong University, Xi'an, Shaanxi, China. [13]Key Laboratory for ImmunoHealth of Shaanxi Province, Xi'an Jiaotong University, Xi'an, Shaanxi, China. [14]These authors contributed equally: Yutiantian Lei, Rui Jia, Chen Chen. ✉e-mail: majinlu@xjtufh.edu.cn; shan87@xjtu.edu.cn; houyuzhu@xjtu.edu.cn